EFFECTS OF PERMAFROST THAW ON TUNDRA CARBON BALANCE OVER SPACE AND TIME

By

ELIZABETH FAY BELSHE

A DISSERTATION PRESENTED TO THE GRADUATE SCHOOL
OF THE UNIVERSITY OF FLORIDA IN PARTIAL FULFILLMENT
OF THE REQUIREMENTS FOR THE DEGREE OF
DOCTOR OF PHILOSOPHY

UNIVERSITY OF FLORIDA

2013

© 2013 Elizabeth Fay Belshe

To my friends Pep Sanjaun, Allie Shenkin, Peter Kelly, Paulo Brando, Caitlin Hicks Pries, Christina Feilding, Jessica Diller

ACKNOWLEDGMENTS

I would like to thank Dr. Ben Bolker for the countless hours of mentoring and support he provided on ecological modeling, which ultimately gave me the confidence and knowledge to understand and analyze the data in my dissertation. Next, I would like to thank Dr. Ted Schuur for his guidance, advice, and endless support throughout my dissertation. I also want to thank Dr. Rosvel Bracho for his help with site-level data analysis and helpful comments and guidance, and thanks to Caitlin Hicks Pries and Pep Sanjuan for allowing me to think out loud and work through my dissertation. Thanks to Forrest Stevens for support with spatial analysis and ArcGIS, Alexander Shenkin for computer and moral support, and Paulo Brando for R support. For valuable field support and ideas during the initial set-up of eddy covariance tower I thank Christian Trucco and Dr. Jason Vogel. Thanks to Sasha Ivans at Campbell Scientific for eddy covariance technical support and training. I would also like to thank UNAVCO for providing GPS equipment, training, and support, which is supported by the National Science Foundation and National Aeronautics and Space Administration under NSF Cooperative Agreement No. EAG-0735156. Finally, I would like to thank the Department of Energy, Graduate Research Environmental Fellowship for support during the last three years of my dissertation.

TABLE OF CONTENTS

page

LIST OF TABLES

LIST OF FIGURES

Abstract of Dissertation Presented to the Graduate School
of the University of Florida in Partial Fulfillment of the
Requirements for the Degree of Doctor of Philosophy

EFFECTS OF PERMAFROST THAW ON TUNDRA CARBON BALANCE OVER SPACE AND TIME

By

Elizabeth Fay Belshe

May 2013

Chair: Edward Schuur
Major: Botany

Climate induced changes to permafrost are altering high latitude landscapes in ways that could increase the vulnerability of the vast soil carbon pools of the region. Thawing of permafrost is a heterogeneous process that creates a complex landscape. In addition to the thickening of soil active layers, localized thermokarst features form when ice-rich permafrost thaws and the ground subsides. By performing a supervised classification on a high-resolution IKONOS image, I detected and mapped small, irregular thermokarst features occurring within an upland watershed in Interior Alaska. Twelve percent of the Eight Mile Lake (EML) watershed has undergone thaw and thermokarst predominantly form in valleys where tussock tundra resides. By incorporating spatial variation created by permafrost thaw into an eddy covariance carbon estimate, I estimated the carbon balance of tundra containing thermokarst. During the two 6-month periods measured, permafrost thaw increased the amplitude of the carbon cycle by stimulating both carbon release and sequestration, while the ecosystem remained a carbon sink at the landscape scale.

To put these results into context and determine if tundra ecosystems were carbon sources or sinks, I compiled 40 years of CO_2 flux observations from 54 studies spanning 32 sites across northern high latitudes. Using time-series analysis, I investigated if seasonal or annual CO_2

fluxes have changed over time, and whether spatial differences in mean annual temperature could help explain temporal changes in CO_2 flux. Growing season net CO_2 uptake has definitely increased since the 1990s; the data also suggest (albeit less definitively) an increase in winter CO_2 emissions, especially in the last decade. In spite of the uncertainty in the winter trend, we estimate that tundra sites were annual CO_2 sources from the mid-1980s until the 2000s; and data from the last seven years show that tundra continues to emit CO_2 annually. CO_2 emissions exceed CO_2 uptake across the range of temperatures that occur in the tundra biome. Taken together, these data suggest that despite increases in growing season uptake, tundra ecosystems are currently CO_2 sources on an annual basis.

CHAPTER 1
INTRODUCTION

Permafrost

A defining characteristic of many high latitude ecosystems is the presence of permafrost, which occurs within 24% of the land area in the northern hemisphere (Anisimov & Nelson 1996; Brown *et al.* 1998). Permafrost is defined as any earth material that remains at or below 0ºC for two or more consecutive years. Since permafrost ground is determined by temperature and not substrate material, it can encompass a wide range of material from solid rock, to mineral and organic soil, to ice (Davis 2001). The surface zone of permafrost that thaws during the summer and completely refreezes during the winter is defined as the active layer (Shur *et al.* 2005). This active layer ranges from a few tens of centimeters to more than several meters thick (Davis 2001). Although active layer thickness is largely controlled by regional climate, other factors such as topographical aspect, vegetation, substrate, and organic matter insulation, and heat conductance of the overlying soil also play a role in determining the extent of seasonal thaw. Global permafrost distribution falls into two broad zones dictated by climate: the zone of continuous permafrost where climate is favorable to permafrost formation and stability, and the zone of discontinuous permafrost where climate is neutral to permafrost and it can be either present or absent depending on local conditions (Shur & Jorgenson 2007). Because climate is dynamic, the distribution of permafrost is continuously changing to be in equilibrium with contemporary climate.

While climate is the dominate factor that determines the geographic extent of permafrost, ecosystem level processes such as soil development, vegetation succession, and disturbance interact to affect the stability and distribution of permafrost (Shur & Jorgenson 2007). Permafrost that forms under favorable conditions consists of a continuous subsurface layer overlain by a

very thick active layer. Ecosystem level processes, such as vegetation changes and soil development, can then act upon and modify the upper permafrost. During ecosystem succession, vegetation cover increases and organic matter accumulates, which in turn buffers the permafrost from air temperatures and results in the upward movement of the permafrost table. This thinning of the active layer is accompanied by an accumulation of ice, which forms an ice-rich intermediate layer between the active layer and permafrost. This ecosystem modified permafrost is more thermally stable because of the protective organic layer but more susceptible to thaw because of its high ice content (Shur & Jorgenson 2007).

Permafrost and Carbon

Carbon is incorporated into permafrost by mechanisms that redistribute it away from the surface to deeper in the soil profile. Organic carbon is initially added to the soil by primary producers and factors such as rooting depth of plants determine the initial depth distribution of new carbon inputs (Schuur *et al.* 2008). Then, inputs to the soil, from either organic matter deposition or various sedimentation processes, cause soil surface accretion. This causes a vertical increase in the soil surface and an upward movement of the permafrost table, which results in organic matter at the bottom of the active layer becoming incorporated into the permafrost (Schuur *et al.* 2008). In addition, cryoturbation (physical mixing of soil horizons that occurs during freeze-thaw processes) helps to move organic matter down into the permafrost (Michaelson *et al.* 1996). These processes result in a variety of organic matter substrates (from labile to recalcitrant) becoming incorporated into permafrost. Then many factors including temperature, hydrology, and substrate quality interact to stabilize carbon in these soils (Hobbie *et al.* 2000). The total permafrost soil carbon pool in the northern circumpolar zone is estimated to be 1672 Pg, which is twice the size of the atmospheric carbon pool (Schuur *et al.* 2008; Tarnocai *et al.* 2009).

Future of Permafrost

Global surface air temperature has increased 0.35 °C decade^{-1} since the 1970's, with dramatic increases since the 1990's (Polyakov *et al.* 2002; Hinzman *et al.* 2005; Serreze & Francis 2006; Euskirchen *et al.* 2007) and temperatures are predicted to rise by up to 6.5 ºC in northern high latitudes by the year 2100 (IPCC 2007). It is estimated that 25-90% of areas with near-surface permafrost will transition to seasonally frozen ground by the year 2100 (Anisimov & Nelson 1996; Saito *et al.* 2007; Lawrence *et al.* 2008; Jafarov *et al.* 2012). In addition, the rate and areal extent of permafrost thaw has already begun to increase (Camill 2005; Hinzman *et al.* 2005; Jorgenson *et al.* 2006; Schuur *et al.* 2008; Osterkamp *et al.* 2009; Romanovsky *et al.* 2010), and active layer thickening has been observed (Zhang *et al.* 2005).

As mean near surface temperatures approach and cross the 0˚C threshold both the geographic extent of permafrost and active layer thickness are expected to change (Anisimov *et al.* 2007). But it is difficult to infer changes in permafrost from changes in air temperature because various disturbances and feedbacks with hydrology, vegetation, and geomorphology complicate the response of permafrost to warming (Stieglitz *et al.* 2003; Grosse *et al.* 2011). And in addition to regional level changes in permafrost distribution and active layer thickness, there can also be localized permafrost degradation that results in thermokarst formation. Thermokarst topography forms when ice-rich permafrost thaws, ground ice melts, surface and subsurface drainage occurs and the ground surface subsides due to volume loss during ice-water phase transition (Hinzman *et al.* 2005). The amount of settlement is dependent on the amount and types of ice that occur in the permafrost, which in turn is dependent on the slope, soil texture, hydrology, vegetation, and climatic and geologic history of the area. So, at the landscape scale there can be a wide diversity of thermokarst features because of differences in local conditions (Jorgenson & Osterkamp 2005). Because of these complex interactions and the diversity of

permafrost composition, the predictability of permafrost thaw and thermokarst formation is a formidable challenge.

Changes in Permafrost and Implications for the Global Carbon Cycle

Permafrost thaw could result in a strong positive feedback to climate change if a portion of the estimated 1670 Pg of soil organic carbon stored in permafrost regions is released to the atmosphere (Schuur *et al.* 2008; Tarnocai *et al.* 2009). The future carbon balance of high latitude ecosystems is dependent on the sensitivity of biological processes (photosynthesis and respiration) to the physical changes occurring with permafrost thawing. Higher soil temperatures increase active layer thickness and create thermokarst terrain, which can change soil hydrology and in turn can either increase or decrease gross primary production and ecosystem respiration. The balance between these large opposing fluxes will depend on the cumulative effect of the landscape level physical changes that occur with permafrost thaw. Therefore, to understand the effects of climate change on the rate and magnitude of carbon exchange, we must quantify both the effects of permafrost thaw on carbon fluxes and the spatial distribution of thaw features, such as thermokarst, across the landscape.

The objectives of this dissertation are to: 1) develop methodology to detect and classify typical thermokarst features occurring in an upland tundra watershed, 2) quantify the effect of permafrost thaw and thermokarst on carbon exchange of an upland tundra ecosystem; and 3) using meta-analysis, assess whether seasonal or annual carbon fluxes within the tundra biome have changed over the past four decades as a result of changes already occurring in high latitude regions.

CHAPTER 2
QUANTIFICATION OF UPLAND THERMOKARST FEATURES WITH HIGH RESOLUTION REMOTE SENSING

Background

Temperature is increasing in northern high latitudes in response to the radiative forcing associated with increasing greenhouse gases and changes in albedo (Chapin *et al.* 2005). Surface air temperature has increased 0.35 °C decade^{-1} since the 1970's, with dramatic increases since the 1990's (Polyakov *et al.* 2002; Hinzman *et al.* 2005; Serreze & Francis 2006; Euskirchen *et al.* 2007) and temperatures are predicted to rise by up to 6.5 ºC in northern high latitudes by the year 2100 (IPCC 2007). This warming affects the spatial distribution of permafrost, which currently occurs within 24% of the ice-free land area in the northern hemisphere (Zhang *et al.* 1999). It is estimated that 25-90% of areas with near-surface permafrost will transition to seasonally frozen ground by the year 2100 (Anisimov & Nelson 1996; Saito *et al.* 2007; Lawrence *et al.* 2008; Jafarov *et al.* 2012), and rate and areal extent of permafrost thaw has already begun to increase (Camill 2005; Hinzman *et al.* 2005; Jorgenson *et al.* 2006; Schuur *et al.* 2008; Osterkamp *et al.* 2009; Romanovsky *et al.* 2010). This thaw could result in a strong positive feedback to climate change if a portion of the estimated 1670 Pg of soil organic carbon in permafrost regions is released to the atmosphere (Schuur *et al.* 2008; Tarnocai *et al.* 2009).

Understanding the relationships among warming, permafrost thaw, and carbon cycling is a challenge because permafrost thaw is temporally dynamic and spatially heterogeneous. Various disturbances and feedbacks with hydrology, vegetation, and geomorphology additionally complicate the response of permafrost to warming (Grosse *et al.* 2011). In addition to the

---

Belshe EF, EAG Schuur, G Grosse (submitted) Quantification of upland thermokarst features with high resolution remote sensing. Environmental Research Letters.

predicted thickening of the active layer (seasonally-thawed surface layer) (Anisimov *et al.* 2007), thawing of ice-rich permafrost can result in thermokarst formation (Hinzman *et al.* 2005; Jorgenson & Osterkamp 2005). Thermokarst landforms often have very different physical and biogeochemical environments compared to the surrounding un-affected permafrost landscape, with impacts on both rates of carbon uptake and emission (Walter *et al.* 2007; Vogel *et al.* 2009; Lee *et al.* 2010; Belshe *et al.* 2012; Jones *et al.* 2012). Ultimately, net landscape-scale carbon exchange will depend on the cumulative response of the mosaicked landscape created by permafrost thaw. Therefore, to estimate the rate and magnitude of carbon efflux from the landscape it is imperative to quantify the size and distribution of thermokarst landforms.

The wide diversity of thermokarst features depends on local permafrost and ground ice conditions, landscape position, hydrology, soil texture, and surrounding vegetation (Jorgenson & Osterkamp 2005). Sixteen primary modes of surface permafrost degradation have been identified, ranging from features with substantial thaw settlement (2-20 m) such as glacial thermokarst and drained lake basins to features with relatively low subsidence (0.2-2 m) such as thermokarst gullies and non-patterned thawed ground (Jorgenson & Osterkamp 2005). One of the major limitations for estimating the size, number, and spatial distribution of thermokarst features is attaining adequate spatial coverage because high latitude ecosystems are vast, isolated, and often inaccessible. Remote sensing allows us to observe these areas in a cost-effective manner and on the timescales needed to answer questions about the rapidly changing landscape. So far, the remote detection of thermokarst has been limited to relatively large and visually distinct features, such as thermokarst lakes (Jones *et al.* 2011; Morgenstern *et al.* 2011), drained lake basins (Hinkel *et al.* 2003; Wang *et al.* 2012), retrogressive thaw slumps (Lantuit & Pollard 2008; Lantuit *et al.* 2012), and thermo-erosion gullies (Godin & Fortier 2012). However,

to capture the true magnitude of thermokarst, it is also necessary to expand observation capabilities towards detection of small, subtle thermokarst forms. With recent advancements in spectral and spatial resolution this is becoming possible.

The objective of this study is to assess the feasibility of very high resolution remote sensing for detecting small irregular thermokarst features (pits, gullies, and long water tracks) in an upland permafrost area in the discontinuous permafrost zone where such features are numerous. Similar thermokarst gullies and pits occur throughout the ~64,000 ha Toklat Basin that extends 80 km to the west of our study site in Interior Alaska, and in many other high-latitude upland areas. By performing a land cover classification targeting thermokarst features in IKONOS satellite imagery, we quantified the spatial extent of thermokarst and determine their spatial distribution and landscape position. Using this information, along with field observations of thaw depth and organic soil depth, we exemplarily assess the vulnerability of soil carbon pools in a typical upland area in the discontinuous permafrost zone of Interior Alaska.

Material and Methods

Site Description

Our study site is the Eight Mile Lake (EML; 63º 52' 42"N, 149º15' 12’’W) watershed and adjacent hill slopes located in the northern foothills of the Alaska Range near Denali National Park and Preserve, Interior Alaska (Schuur *et al.* 2007; Schuur *et al.* 2009). The study areas covers 10.4 km^2 and is located at ~700m elevation on a gently sloping (~5%), north facing glacial terminal moraine that dates back to the Early Pleistocene. Nenana gravel constitutes the major bedrock formation of the area and due to multiple glacial advances and retreats a landscape of rolling hills and valleys has formed (Wahrhaftig 1958). The hilltops have gravelly soils associated with glacial till and are covered by a thin aeolian silt cap, while the lower slopes

and valleys have thick peat accumulations over fine-grained soils associated with colluvial deposits (Osterkamp *et al.* 2009).

The study area is underlain by permafrost but it is also mapped within the vulnerable band of discontinuous permafrost near the point of thaw due to the combination of its elevation and geographic position (Yocum *et al.* 2006; Romanovsky *et al.* 2007). Permafrost at EML is classified as climate-driven, ecosystem protected (Shur & Jorgenson 2007) because the permafrost was formed under an earlier cold climate independent of ecological conditions and later protected from degradation by vegetation and soil development (Osterkamp *et al.* 2009). The long-term mean annual air temperature (1976-2009) of the area is -1.0 °C and the growing season mean temperature is 11.2 °C, with monthly averages ranging from -16 °C in December to +15 °C in July. The long-term annual precipitation is 378 mm with a growing season precipitation of 245 mm (National Climatic Data Center, NOAA). Deep permafrost temperature has been measured in a borehole at the site since 1985 and during this time mean annual ground temperature rose by 1°C (1989-1998) and thermokarst terrain has developed and expanded (Osterkamp *et al.* 2009).

Land Cover Classification

Image acquisition and field sampling

A multi-spectral IKONOS satellite image covering the EML watershed and adjacent hillslope was collected on the 25th June 2008 (Figure 2-1). IKONOS Geo[1] products have a spatial resolution of 3.2 meters for multispectral bands with a position accuracy of 5±3 meters. To improve this georectification, eleven ground control points collected in the field with a differential global positioning system (DGPS), along with nearest neighbor resampling and a 2nd order polynomial transformation were used to rectify the image, achieving an average root mean square error (RMSE) of 0.98 meters.

Information on vegetation and soil was collected within 8 *a priori* selected land cover types (2-1). An unsupervised classification of the IKONOS image was used to aid in selection of these potential classes along with field knowledge of the study area. Our sampling strategy focused on spatial coverage, therefore rapid assessment quantification metrics were used. Approximately 10 field training sites were sampled within each class, resulting in a total of 78 training sites distributed throughout the watershed (Table 2-1, Figure 2-1). At each site, four contiguous (2x2 m) plots were established within homogeneous areas that were representative of the site's vegetation. Within each plot, the percent of ground cover (vegetation, water, bare soil) was estimated and geographic location was taken with DGPS. Vegetation was further categorized by the percent cover of functional groups (graminoid, herbaceous, non-vascular, shrub, tree) and percent cover of each species. Due to identification difficulties and time limitations, *Salix spp., Alnus spp., Dicranum spp.* and *Sphagnum spp.* were only identified to genera and rare non-vascular plants were grouped into a non-vascular "other" category. These data were used to further characterize the eight land cover types (table 1), which we compared to the Denali landcover mapping project (DLMP; Stephens *et al,* 2001) and the Circumpolar Arctic vegetation map (CAVM; Walker *et al,* 2005). At the end of the growing season (late August) active layer thickness (depth to permafrost) was measured at each site by inserting a metal rod until the impermeable permafrost layer was reached. Differences in thaw depth among land cover classes were evaluated using an ANOVA with a Tukey post-hoc test and analysis was performed in R (R Core Development Team 2011). In addition, depth of the near-surface organic horizon was measured in small soil pits dug at each site. Because deep organic horizons (40-60cm) occurred in some classes and due to field time limitations, pits were only dug to ~20 cm.

If the organic horizon extended below 20 cm the site was considered highly organic and grouped into a >20 cm category.

Fine scale differences in elevation of the study area were measured with a survey-grade DGPS. One GPS unit (Trimble 5400) was placed at a nearby USGS geodetic marker (WGS84, 63°53'16.56"N, 149°14'17.92"W), which acted as the reference receiver. Using a second GPS unit (Trimble 5400) secured to a backpack, a kinematic survey was conducted by walking transects of the 10.4 km study site. Geographic position and elevation were collected at 5 s intervals, yielding a total of 68,000 data points. These data were post processed with methodology developed by UNAVCO using Trimble Geomatics Office software (Dayton, Ohio).

Data preparation

A combination of DGPS point measurements of elevation and USGS Hydrologic Line Graphs Maps were used to create a digital elevation model (DEM) with 5 m grid cell size of the study area with the Topo to Raster function in the 3D Analyst Tool of ArcGIS 9.3. Slope was derived from the resulting DEM after it was smoothed using mean focal statistics (10 x 10 cell rectangle) with the Spatial Analyst tool in GIS. IKONOS bands 3 and 4 were used to calculate the normalized difference vegetation index (NDVI), which is a measure of photosynthetically active vegetation and can be used as an indicator for "greenness" and productivity (e.g., (Raynolds *et al.* 2006). We expected that NDVI could potentially help separate thermokarst classes because vegetation within thermokarst at our study site has been shown to have higher productivity than surrounding tussock tundra (Schuur *et al.* 2007). To reduce the spectral overlap between some training classes, we also performed a principal components analysis (PCA) on IKONOS bands 1-4. Based on visual inspection of spectral separation, we used the first three PCA bands in subsequent analysis.

Supervised classification

For the final classification we combined six data layers (PCA1, PCA2, PCA3, NDVI, elevation, slope) and performed a maximum likelihood classification based on spectral signatures of the training sites. The spectral separability of individual training data were visually evaluated in scatter plots combining the different data layers. Classes were merged if their spectra appeared to have insufficient separation. Originally the spruce, alder and willow classes were evaluated independently, but because they spectrally were very similar they were merged into a mixed riparian class. Post classification majority filtering was done to remove small numbers of pixels within larger contiguous classes and to achieve a smoother final classification. All classification analysis was done with ERDAS Imagine 9.1 software (Atlanta, GA).

Classification accuracy assessment

Independent validation sites representative of each land cover class were collected during the field campaign in 2009 (78 sites total; ~10 within each class) and from high-resolution true-color aerial images taken of the watershed in 2003 (203 total). Cross-tabulated error matrices of the mapped classes and validation sites were used to assess classification accuracy (Congalton & Green 1999) and estimate overall accuracy, user's and producers accuracies, and the Kappa statistic. The producer's accuracy indicates the probability of a reference pixel being correctly classified (omission error), while the user's accuracy is the probability that a pixel on the map accurately represents that category on the ground (commission error). The Kappa statistic incorporates the off-diagonal elements of the error matrices (i.e. classification errors), which represents agreement obtained after removing the proportion that could be expected by chance (Jensen 2005).

Results

The EML watershed grades in elevation from 680 m in the south to 632 m in the north, where the lake is situated. Superimposed upon this overall gradient in elevation are rolling hills and valleys that differ in elevation by roughly 15 m. The final thematic map derived from the supervised classification shows that hilled areas correspond with the Hilltop Shrub (HS) class, which transition to the tussock tundra (TT) class found in the valleys (Figure 2-2). The two classes associated with permafrost degradation (Thermokarst, TK, and Thermokarst Pool, TP) mainly occur in the valleys of the watershed within the tussock tundra class (Figure 2-2). In general, thermokarst features at EML are elongated (~ 300 -700 m), slightly incised (<1 m) gullies that drain from the valleys towards the lake (see inset of Figure 2-2 for a close-up of typical thermokarst patterns). On average, ground subsidence within thermokarst features is less than 1 meter, and while individual gullies are relatively narrow (1-5 m wide), aggregated together they can affect areas up to 75 m wide (Figure 2-2). The mapped thermokarst classes combined (TK and TP) cover 1.31 km^2, which is 12.1 % of the 10.4 km^2 study area (Table 2-2). Tussock tundra (TT) covers 2.4 km^2 (22.9% of the total area), Hilltop shrub (HS) covers 1.7 km^2 (15.8%), Shrub Tundra Transition (ST) covers 2.3 km^2 (22%), and the Mixed Riparian (MP) covers 2.2 km^2 (21%; Table 2-2). Assuming that the thermokarst areas originally were all covered with tussock tundra, we estimate that the unthawed tussock tundra originally covered 3.7 km2 and by 2008 approximately 1/3 (34.6%) had undergone permafrost thaw.

All training sites of thermokarst classes (TK, TP) and tussock tundra (TT) had soil organic layers greater than 20 cm thickness, while all other classes had organic layers shallower than 20 cm (Figure 2-3). Our field method of categorizing all training sites with organic layers >20 cm as highly organic does not allow us to statistically differentiate between classes because we did not measure variance within sites with thick organic layers due to the challenge of

sampling into frozen soil with limited field time. However, previous work in the same watershed reported that soil organic layers range from 37±3.1 cm at minimally thawed tundra sites to 54±4.8 cm at extensively thawed sites (Hicks Pries *et al.* 2012). These site-specific data along with our field data across the watershed show that permafrost subsidence at EML is occurring in areas with relatively large soil organic layers.

Thermokarst classes (TK, TP) have greater maximum seasonal thaw depths than other land cover classes (Figure 2-4). On average, thaw depth within TK and TP classes was 73 and 85 cm, respectively. The Mixed Riparian class (RM) did have a few sites near the lake inlet that exhibited deep thaw depths (66 & 81 cm), but on average all other land cover classes had thaw depths of 44 cm or lower. RM sites near the lake inlet most likely exhibited deeper thaw depths due to the thermal influence of a thaw bulb developing beneath the lake. Notably, the tussock tundra (TT) class had much lower and less variable thaw depths than the thermokarst classes, even though they are adjacent to each other. This confirms that soils within thermokarst are seasonally thawing to a greater extent than any other land cover class.

The overall classification accuracy of the IKONOS image was 83%, and there was adequate agreement between the final map and training data (Kappa value of 0.79). The user's and producer's accuracies of individual classes were consistently high, ranging from 69% to 100% (Table 2-3). Thermokarst classes had a producer's accuracy of 79% and 83% and a user's accuracy of 75% and 100%, for TK and TP classes respectively. For the thermokarst classes, the highest confusion occurred between the TK and ST class, with 15% of TK training pixels being classified as ST. This misclassification most likely occurred because sloped sites within the TK class have very similar vegetation compositions as the ST class. Both are dominated by short stature shrubs and have similar species compositions (Table 2-1). Previous work at EML has

shown that the vegetation composition shifts from tussock-forming sedges to shrubs as thermokarst develop (Schuur *et al.* 2007). This is similar to the vegetation change that occurs at the transition between tussock tundra valleys and shrubby hilltops. The other obvious misclassification occurred between the MR and HS classes, with 31% of MR training pixels classified as HS (Table 2-3). We believe this confusion occurred because the MR class is a mosaic of vegetation types that include tall shrubs that are spectrally similar to the medium stature shrubs occurring on the hilltops. Additionally, the classification was not well resolved in the southern portion of the watershed and overestimates the homogeneity and dominance of the RM class at the southern tip. This incongruity was caused by the low number of training sites in this steeply sloped region. However, we achieved an overall acceptable accuracy, with thermokarst classes having comparable accuracy to other classes in the landscape.

Discussion

Twelve percent of the landscape within EML watershed has undergone permafrost thaw resulting in thermokarst formation (Table 2-2). Although thermokarst features are widespread throughout the watershed, they predominately occur within the low-lying valleys dominated by tussock tundra (Figure 2-2). This pattern of ground subsidence is dictated by the initial amount and distribution of ice-rich permafrost, which in turn resulted from the geology and soils of the area. The EML watershed experienced multiple glacial advances and retreats that created a landscape of rolling hills and valleys (Wahrhaftig 1958). The hills have gravelly soils consisting of glacial till covered by a thin aeolian silt cap with low amounts of ice within the permafrost. Alternatively, the lower slopes and valleys have fine-grained soils associated with colluvial deposits and ice-rich horizons containing up to 50% visible ice content (Osterkamp *et al.* 2009). These ice layers and lenses formed over time as peat accumulated in the valleys and water was trapped by upward freezing of the permafrost surface (Osterkamp *et al.* 2009). Although the peat

accumulations initially acted to build and protect the permafrost, the concurrent increase in ice ultimately made permafrost in the valleys vulnerable to thermokarst formation. Through continued warming, insulation of soil by snow accumulating in subsided areas, and thermal erosion (from water being redistributed from higher to lower microtopographical areas) permafrost thaw has increased and thermokarst gullies and pools have expanded (Kane *et al.* 2001; Osterkamp *et al.* 2009). Based on our land cover classification dendritic patterns of thermokarst gullies have formed throughout the valleys of the watershed. We estimate approximately 1/3 of the original 3.7 km^2 tundra land cover class has undergone near-surface permafrost thaw that resulted in thermokarst formation. It is important to note that this is likely an underestimate of total permafrost degradation since thawing that does not result in subsidence (such as the deepening of active layers) may not be remotely detected.

Thermokarst and tussock tundra classes occur in areas with relatively thick soil organic layers compared to other land cover classes within the EML watershed (Figure 2-3). Although our soil data is semi-quantitative where we did not quantify variability >20 cm, previous intensive work within tundra at EML reports soil organic layers range from 37-54 cm (Hicks Pries *et al.* 2012; sites occur within the subset of Figure 2-2). At these same sites, carbon inventories of the top meter of soil ranged from 55 to 69 kg C m^{-2}, which is on the upper end of the range (16-94 kg C m^{-2}) reported for similar tundra soils across Alaska (Michaelson *et al.* 1996). They also found no difference in carbon pools at minimally and extensively subsided tundra sites (Hicks Pries *et al.* 2012). By extrapolating this intensive plot data, we estimate that both tundra and thermokarst classes have organic soil layers that are twice as deep as other classes in the watershed. In spite of the thermal protection provided by the extensive organic soil accumulations in the valleys (Shur & Jorgenson 2007), under present climate conditions, this

protection is no longer sufficient to keep the underlying near-surface permafrost from thawing and thermokarst from forming and expanding.

The soil profile of thermokarst classes is seasonally thawing to a greater extent than any other land cover class, and thaw depth in thermokarst is twice as deep as in the surrounding tussock tundra (Figure 2-4). This increase in thaw depth results from convection as water is redistributed into subsided areas as well as increases in soil thermal conductivity as organic matter becomes saturated. Both of these processes increase ground heat flux within depressions while decreasing heat flux in higher, dryer areas (Jorgenson *et al.* 2001; Kane *et al.* 2001; Bonan 2002; Yoshikawa & Hinzman 2003; Jorgenson & Osterkamp 2005; Osterkamp 2005; Osterkamp *et al.* 2009). The net result is deeper thawing in subsided, saturated areas and a decrease in thaw in the high relief areas of the adjacent tundra from which water is drained. This pattern of increased thaw depth within subsided areas has been widely documented at EML (Vogel *et al.* 2009; Lee *et al.* 2010; Belshe *et al.* 2012; Trucco *et al.* 2012).

The landscape level changes created by permafrost thaw within the EML watershed have important implications for its carbon cycle because thermokarst features are forming in the valleys soils rich in organic carbon and are altering the physical environment in ways that increase the vulnerability of the soil carbon pool. Through associated changes in temperature and hydrology, thermokarst causes the active layer of soil to thaw to a greater extent. This exposes more previously frozen organic carbon to above-freezing temperatures and extends the time it remains unfrozen because it takes longer to refreeze the greater volume of unfrozen soil. These abiotic changes can stimulate decomposition and nitrogen mineralization, and result in increased carbon emissions, unless buffered by changes in soil hydrology (Shaver *et al.* 1992; Goulden *et al.* 1998; Davidson & Janssens 2006; Schuur *et al.* 2008). On the other hand, thermokarst

formation can lead to increased carbon uptake if decomposition increases plant available nitrogen (Chapin & Shaver G. 1996; Hobbie *et al.* 2000; Mack *et al.* 2004), or the plant community shifts to more highly productive species (Schuur *et al.* 2007; Osterkamp *et al.* 2009).

Currently, tundra undergoing permafrost thaw at EML is a carbon source on an annual basis, emitting on average 54 g C m^{-2} $year^{-1}$ over the past few years (2008-2010; (Belshe *et al.* 2012). Although both growing season net carbon uptake and winter carbon emissions have increased in conjunction with ground subsidence at EML (Vogel *et al.* 2009; Trucco *et al.* 2012), growing season net sink activity is negated by winter carbon emissions (Belshe *et al.* 2012). We believe this current imbalance is created because decomposition can continue to increase as permafrost thaw exposes more of the vast soil organic pool, while the magnitude of potential carbon uptake is mediated by size limitations of species currently residing in the tundra. This trajectory will continue as more soil is exposed with thaw, unless offset in the future, on the timescale of plant succession, by boreal trees advancing from the mixed riparian land cover class into the tundra. An important next step is to build upon this analysis to detect changes in thermokarst extent as well as shifts in vegetation cover with remote sensing image time series.

Concluding Remarks

Using a supervised maximum likelihood classification approach and a very high resolution IKONOS image, we detected and mapped small, irregular thermokarst features occurring within the EML watershed (Figure 2-2). Overall we achieved an acceptable classification accuracy of 83%, with thermokarst classes having comparable accuracy to other classes in the landscape (Table 2-3). Our analysis shows that twelve percent of the landscape at EML has undergone subsidence, and thermokarst induced physical changes have important implications for the carbon balance of this ecosystem. The considerable time and work necessary to collect ground truth data within our relatively small (10.4 km^2) study area indicate that

mapping of such thermokarst features remains challenging despite their importance for understanding and projecting tundra ecosystem transitions. Homogeneous very high resolution remote sensing data will be useful to investigate such features in other areas. However, we believe that only a combination of very high resolution imagery and elevation data, such as from LIDAR, will allow successful mapping of such small, but widespread upland thermokarst features over larger study regions. With the horizontal resolution (15-30m) and vertical accuracy (>5-10 m) of most digital elevation models currently available in high latitude areas, it is not possible to extend this type of analysis to larger areas. Consequently, advances in other spatial products are needed, in conjunction with high-resolution images, to detect formation of small thermokarst features that form due to climate or disturbance induced changes in high latitude ecosystems.

Table 2-1. Characterization of land cover classes and the number of field training sites used for the supervised classification.

Land Cover Class	Training sites	Description
Hilltop Shrub (HS)	10	Hill top communities dominated (85%) by medium stature (60-120 cm) shrubs (*Betula nana, Betula glandulosa*). *Similar to DLMP land cover class closed low shrub birch. §Similar to the CAVM land cover class S2 low shrub tundra.
Shrub Tundra Transition (ST)	10	Intermediate transition zone between hilltops and valleys with intermediate stature (25-55 cm) vegetation that is a mixture of shrubs (63%; *Betula nana*, *Rubus chamaemorus*, *Rhododendron groenlandicum*, *Empetrum nigrum*, *Vaccinium vitis-idaea*, *Vaccinium ulginosum*), graminoids (16%; *Eriophorum vaginatum*, *Carex bigelowii*) and non-vascular (17%; *Dicranum spp.*, *Sphagnum spp.*, Feather-moss, Lichen) plants. §Similar to the CAVM land cover class S2 low shrub tundra and G4 tussock-sedge, dwarf-shrub, moss tundra.
Tussock Tundra (TT)	10	Mixture of short stature (>25 cm) graminoid (35%; *Eriophorum vaginatum*, *Carex bigelowii*), shrub (38%; *Betula nana*, *Rubus chamaemorus*, *Rhododendron groenlandicum*, *Empetrum nigrum*, *Vaccinium vitis-idaea*, *Vaccinium ulginosum*) and non-vascular (25%; *Dicranum spp.*, *Sphagnum spp.*, Feather-moss, Lichen) vegetation occurring in gently sloping valleys. *Similar to DLMP land cover class low shrub sedge. §Similar to the CAVM land cover class G4 tussock-sedge, dwarf-shrub, moss tundra.
Thermokarst Pool (TP)	4	Pools of standing water created by permafrost degradation in areas of low slope. Pools are generally around 5 m wide and less than 50 cm deep.
Thermokarst (TK)	22	Thermokarst gullies that have three types of vegetation depending on the local slope and drainage. Relatively low slope areas are dominated by either non-vascular species (60%; *Sphagnum spp.*) or graminoid species (67%; *Eriophorum spp* ,*Carex bigelowii*), while area with greater slope and drainage are dominated by a mixture of intermediate stature (20-63 cm) shrub species (61%; *Betula nana*, *Rubus chamaemorus*, *Rhododendron groenlandicum*, *Empetrum nigrum*, *Vaccinium vitis-idaea*, *Vaccinium ulginosum*). §Similar to the CAVM land cover class S2 low shrub tundra in high slope areas and W4 sedge, moss, low-shrub wetland in low slope areas.
Mixed Riparian (MR)	18	Mixed vegetation near the inlet and outlet of the lake, and alongside the road. Vegetation is a matrix of patches of needle-leaf trees (*Picea mariana*) and large shrubs (200 - 600cm; either *Salix spp*. or *Alnus spp*.). *Similar to DLMP land cover classes Stunted Spruce, Alder, and Willow. §Similar to the CAVM land cover class S2 low shrub tundra.
Road (RD)	4	Stampede Road. *Similar to DLMP land cover class bare ground.
Lake (LA)	NA	Eight Mile Lake. *Similar to DLMP land cover class clear water.

* Denali Landcover Mapping Project (DLMP); Stephens et al. 2001

§ Circumpolar Arctic vegetation map (CAVM); Walker et al. 2005

Table 2-2. Spatial extent and percent of total area covered by each class within the study area.

Land Cover Class	Area %	Area km^2
Hilltop Shrub (HS)	15.8	1.7
Shrub Tundra Transition (ST)	22.4	2.3
Tussock Tundra (TT)	22.9	2.4
Thermokarst (TK)	12.0	1.3
Thermokarst Pool (TP)	0.1	0.01
Mixed Riparian (MR)	21.0	2.2
Lake (LA)	5.2	0.5
Road (RD)	0.5	0.1
Total Area	100	10.4

Table 2-3. Summary of supervised classification accuracy assessment that includes a confusion matrix of the classification and ground truth data, along with the producer's and user's accuracies (%), the overall accuracy, and the Kappa statistic.

	Ground truth (pixel)										
Land Cover	HS	ST	TT	TK	TP	MR	LA	RD	Total	Producer's	User's
HS	1501	234	0	61	0	166	0	0	1962	85	74
ST	60	3999	216	100	0	7	0	0	4382	69	77
TT	1	126	8624	7	0	0	0	0	8758	97	88
TK	78	538	66	459	0	23	0	0	1164	79	75
TP	0	0	0	2	45	2	2	0	51	83	100
MR	68	4	0	19	0	338	0	0	429	77	90
LA	0	0	0	0	0	0	836	0	836	100	100
RD	0	0	0	0	0	0	5	82	87	100	100
Total	1708	4901	8906	648	45	536	843	82	17669		
Overall Accuracy	83%										
Overall Kappa	0.79										

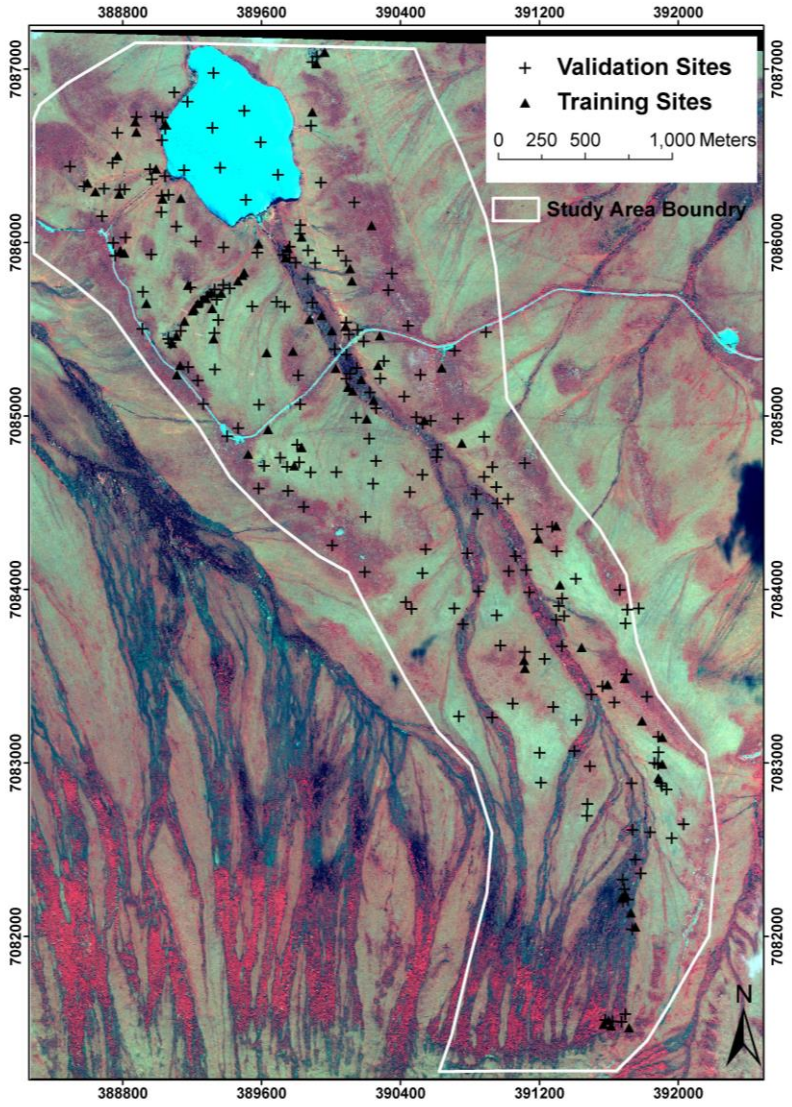

Figure 2-1. IKONOS image taken during June 2008 of the EML watershed and adjacent hill slope (10.4 km^2 study area outlined in white) located in Healy, Alaska. Training sites used for the supervised classification and validation sites used for accuracy assessment are also shown.

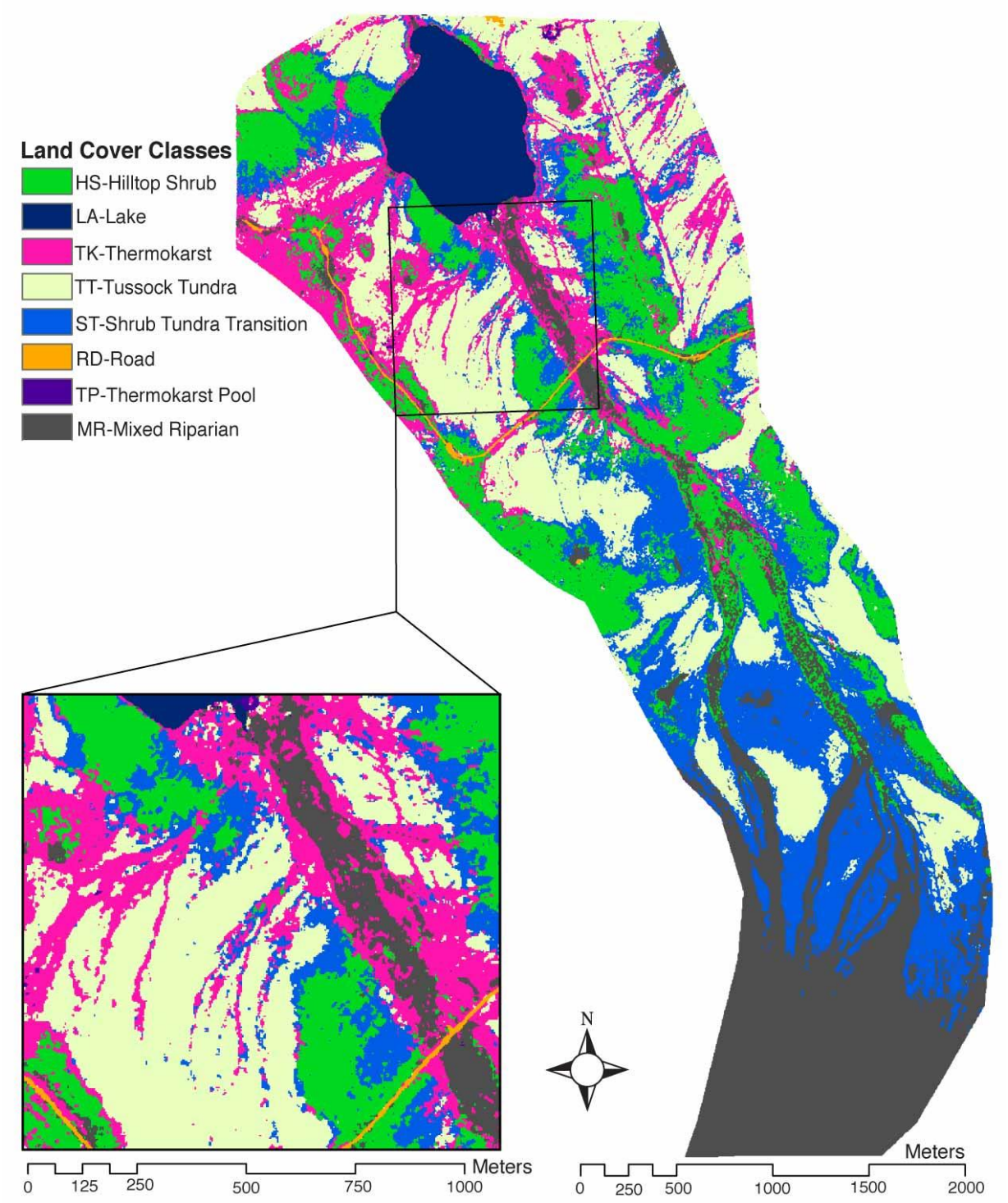

Figure 2-2. Mapped supervised classification of the EML watershed and adjacent hill slope, with a boxed subset showing the area where previous studies measured carbon pools and fluxes.

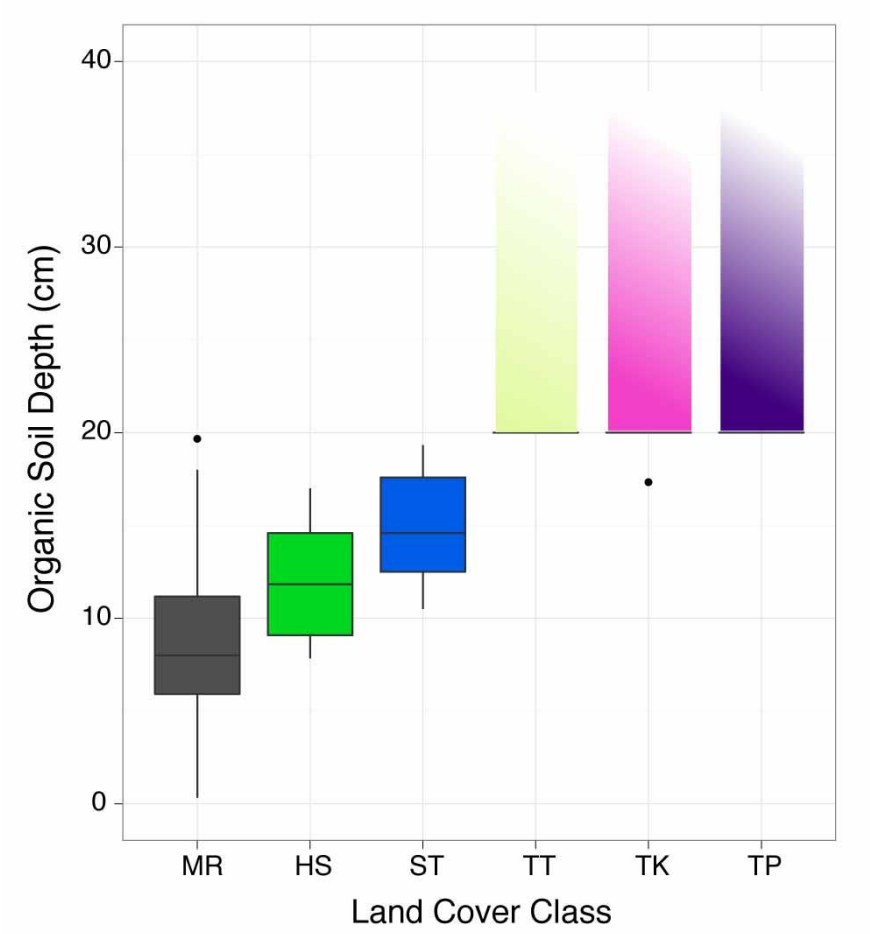

Figure 2-3. Soil organic layer thickness (cm) of land cover classes, with colors corresponding to the mapped supervised classification. Classes with organic depths less than 20 cm (MR, HS, ST) are shown in box-plots, with solid line denoting mean and box denoted the 25th & 75th quartile. Classes grouped into the >20cm category (TT, TK, TP) have boxes that start at 20cm and fade toward 40 cm to represent that previous site measurements show organic depths are greater than 20cm (ranging from 37-54 cm) for these classes.

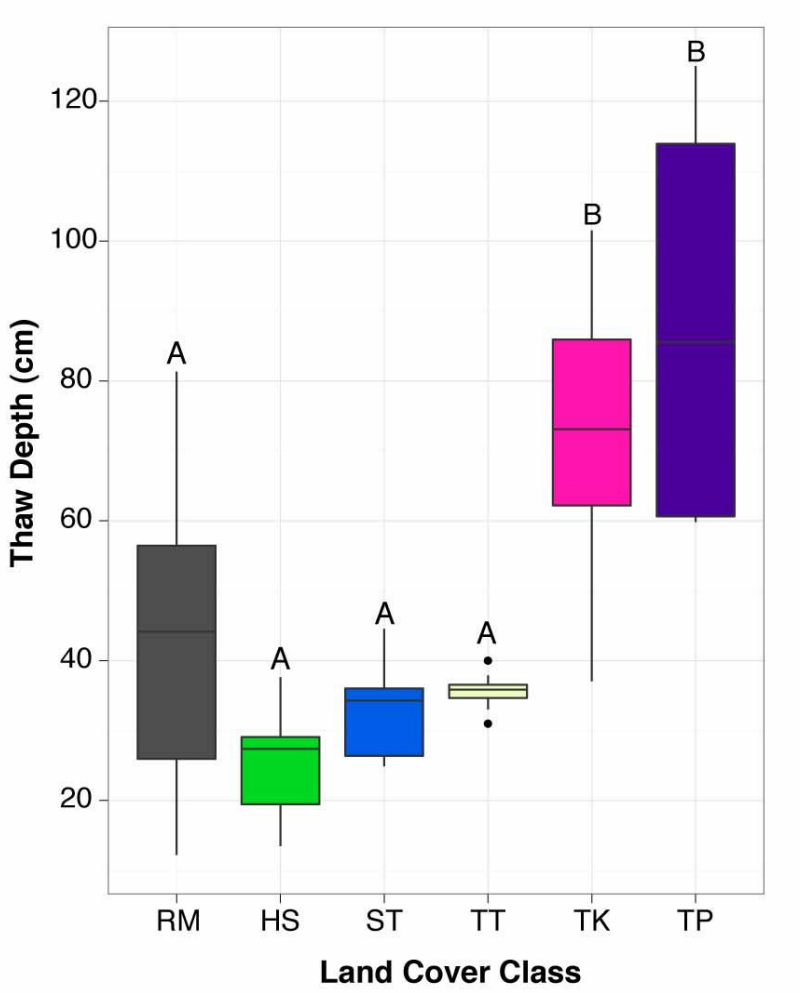

Figure 2-4. Maximum seasonal thaw depth (cm) of land cover classes, with solid line denoting mean and box denoted the 25th & 75th quartile, and colors corresponding to the mapped supervised classification. Letters denote differences among classes at a statistical significance at P≤0.05.

CHAPTER 3
INCORPORATING SPATIAL HETEROGENEITY CREATED BY PERMAFROST THAW INTO A LANDSCAPE CARBON ESTIMATE

Background

Northern high latitudes are disproportionally warming and Arctic temperatures are predicted to increase by 6.5 ºC or more by the year 2100 in response to radiative forcing caused by increasing greenhouse gases and changes in albedo (Chapin *et al.* 2000; Chapin *et al.* 2005; Hinzman *et al.* 2005; IPCC 2007). Currently, permafrost occurs within 24% of the ice-free land area in the northern hemisphere (Zhang *et al.* 1999), and it is estimated 25-90% will degrade into seasonally frozen ground by the year 2100 (Anisimov & Nelson 1996; Saito *et al.* 2007; Lawrence *et al.* 2008). According to recent estimates, permafrost soils contain twice as much carbon (1672 Pg) as the entire atmospheric pool (Schuur *et al.* 2008; Tarnocai *et al.* 2009). If a portion of this C is released to the atmosphere it could result in a strong positive feedback to climate change. Understanding how permafrost thaw affects the rate of C exchange from this large pool is essential for understanding the global C cycle in a warmer world.

Thawing of permafrost is a temporally dynamic and spatially heterogeneous process. Rising temperatures increase active layer (seasonally-thawed surface layer) thickness and form thermokarst (Jorgenson & Osterkamp 2005; Zhang *et al.* 2005). Thermokarst is uneven ground that forms when ice-rich permafrost thaws, drainage occurs, and the ground surface subsides (Jorgenson & Osterkamp 2005). These localized changes in surface relief greatly alter the surface hydrology of the area. As water is redistributed from higher to lower microtopographical areas, thermal erosion by the movement of water warms the soil and further perpetuates

---

Belshe EF, BM Bolker, R Bracho, EAG Schuur (2012) Incorporating Spatial Heterogeneity Created by Permafrost Thaw into a Landscape Carbon estimate. Journal of Geophysical Research: Biogeosciences Vol. 117.

permafrost thawing (Kane *et al.* 2001; Osterkamp *et al.* 2009). This positive feedback creates a mosaic of patches that range from high, dry embankments with shallow active layers to subsided areas with relatively wet, warm soils and deep active layers (Osterkamp *et al.* 2009; Vogel *et al.* 2009; Lee *et al.* 2010). Furthermore, this pattern of ground subsidence, dictated by the initial presence of ice-rich permafrost, is interspersed throughout the landscape and ultimately creates a mosaic of various degrees of permafrost thaw and microtopography.

The future C balance of high latitude ecosystems depends on the sensitivity of biological processes (photosynthesis and respiration) to the physical changes in temperature and moisture occurring with permafrost thaw. But, predicting C exchange in these ecosystems is difficult because of the landscape heterogeneity created as permafrost thaws. Since adjacent patches can have very different physical environments, they can have very different gross primary production (GPP) and ecosystem respiration (R_{eco}) (Vogel *et al.* 2009; Lee *et al.* 2010). Landscape-scale GPP and R_{eco} will depend on the cumulative response of the landscape to permafrost thaw, which in turn will dictate the direction and magnitude of net ecosystem exchange ($NEE = GPP - R_{eco}$).

The response of the C cycle to spatial and temporal environmental variation is often non-linear and not simply described by the mean response (Aubinet *et al.* 2002). Therefore, an appropriate understanding of both the spatial and temporal variation of C flux is essential for estimating the C balance of a landscape. But the intensive temporal sampling required for good estimates of C flux makes it difficult to obtain extensive, spatially explicit C flux data. Eddy covariance (EC) provides a method to directly measure C exchange at a high level of temporal resolution over a large spatial scale (Baldocchi 2003). But fluxes measured by EC are commonly assumed to come from a homogenous surface, which makes it difficult to resolve the cumulative contribution of localized features in the landscape to an EC estimate (Schmid & Lloyd 1998;

Laine *et al.* 2006). Although much effort has gone into developing and using models to locate where fluxes originate (i.e. the footprint of an EC tower) (Schmid 1997; Schmid & Lloyd 1998; Kormann & Meixner 2001; Schmid 2002), less effort has gone into incorporating spatial information back into EC C estimates. However, the abundance of data produced by EC towers gives us the ability to explore spatial patterns of C flux.

In this study, we use generalized additive models (GAMs) to generate a continuous time series of NEE for a tundra landscape undergoing permafrost thaw. We developed a spatially explicit quantitative metric of permafrost thaw based on variation in microtopography. By incorporating our spatial metric into EC gap filling models, we were able to make C flux predictions for the landscape as a whole, as well as for specific landscape patches throughout the continuum of permafrost thaw and ground subsidence. We tested the robustness of our models against more widely used (non-spatial) gap filling methods. Our objectives were to more accurately estimate the C balance of a heterogeneous landscape and to explore the collective effect of permafrost thaw on the plant and soil processes that dictate ecosystem C exchange.

Material and Methods

Site Description

The study site is within the Eight Mile Lake (63º 52' 42"N, 149º15' 12''W) watershed in the northern foothills of the Alaska Range near Denali National Park and Preserve (Schuur *et al.* 2007; Schuur *et al.* 2009). This upland area occurs within a vulnerable band of discontinuous permafrost near the point of thaw due to the combination of its elevation and geographic position (Yocum *et al.* 2006; Romanovsky *et al.* 2007). Deep permafrost temperature has been measured at the site since 1985 and during this time thermokarst terrain has developed and expanded as the permafrost has warmed (Osterkamp *et al.* 2009). Vegetation at the site is dominated by moist acidic tussock tundra comprised of sedge (*Eriophorum vaginatum),* deciduous and evergreen

shrubs (*Vaccinium uliginosum, Rubus chamaemorus, Betula nana and Ledum palustre*), and non-vascular plants (*Sphagnum* spp., *Dicranum* spp., feathermoss and lichens). Soils at the site are classified as Gelisols because permafrost is found within 1 meter of the soil surface (Soil Survey Staff 1999). An organic horizon, 0.45-0.65 m thick, covers cryoturbated mineral soil that is a mixture of glacial till (small stones and cobbles) and windblown loess. Organic C pools in the top meter of soil range between 55-69 kg C m^{-2} (Hicks Pries *et al.* 2012).

The long-term mean annual air temperature (1976-2009) of the area is -1.0 °C and the growing season (May-Sept) mean air temperature is 11.2 °C, with monthly averages ranging from -16 °C in December to +15 °C in July. The long-term annual mean precipitation is 378 mm with a growing season mean precipitation of 245 mm (National Climatic Data Center, NOAA). Mean growing season air temperature was 8.1 °C and 9.7 °C during 2008 and 2009, respectively, and growing season precipitation was 346 mm and 178 mm during 2008 and 2009, respectively.

Eddy Covariance Measurements

NEE was measured using eddy covariance (EC) from June to December 2008 and April to October 2009. The EC system consisted of a CSAT3 sonic anemometer (Campbell Scientific, Logan, UT) and an open path CO_2/H_20 gas analyzer (Li-7500, LI-COR Biosciences, Lincoln, NE) mounted on a 2m tower. Data were recorded at a frequency of 10 Hz on a CR5000 data logger (Campbell Scientific, Logan, UT), and fluxes were Reynolds averaged over 30 min time periods (Reynolds 1985). Calibration was preformed monthly during the growing season using a zero CO_2 air source, a ± 1% standard CO_2 concentration, and a dew point generator (Li-610, LI-COR Biosciences, Lincoln, NE) for water vapor. The EC tower was placed within a patchy landscape consisting of visibly subsided areas to the North and West and relatively even terrain to the South and East. The fetch from the tower was greater than 300 m in all directions and winds predominantly came from the NE and SW. An analytical footprint model developed by

Korman and Meinxner (2001) showed on average 50% of fluxes originated within the first 50 m around the tower, and greater than 80% of fluxes originated within 200 m from the tower.

Eddy Covariance Data Handling

Raw CO_2 fluxes were corrected for damping of high frequency fluctuations, sensor separation, and misalignment of wind sensors with respect to the local streamline (Moncrieff *et al.* 1997; Aubinet *et al.* 2000; Wilczak *et al.* 2001). CO_2 fluxes were then corrected for variations in air density due to fluctuation in water vapor and heat fluxes (Webb *et al.* 1980) and for fluctuations caused by surface heat exchange from the open path sensor during wintertime conditions (Burba *et al.* 2008). Data screening was applied to eliminate half-hourly fluxes with systematic errors and non-relevant environmental influences such as: (1) incomplete half-hour data sets as a result of system calibration or maintenance, (2) time periods when the canopy was poorly coupled with the external atmospheric conditions as defined by the friction velocity, u^* (threshold < 0.12 m s^{-1}; (Goulden *et al.* 1996; Clark *et al.* 1999), (3) excessive variation from the half-hourly mean based on an analysis of standard deviations for u, v, and w wind statistics and CO_2 fluxes. Fluxes were then divided into weekly data sets for both day and night conditions and unrealistic low or high values (>2 standard deviations from the mean) were filtered out. In total, ecosystem fluxes were measured 72% and 96% of the time during the 2008 and 2009 campaigns, respectively, while 64% and 60% of those values were eliminated by the screening criteria listed above. The quality of our data was evaluated by the degree of growing season energy closure (Rnet = LE + H + G), which was 76% in 2008 and 73% in 2009. Ground heat flux (G) was estimated as the change in soil temperature with depth plus soil heat storage (Liebethal *et al.* 2005; Liebethal & Foken 2007). To calculate soil heat storage, we assumed 40% organic matter content (Hicks Pries *et al.* 2012) and 60% volumetric water content based on soil cores taken from the site. Measurements of half-hour NEE were calculated as: NEE = Fco_2 + Fs, where Fco_2

was the mean flux of CO_2 at measurement height and Fs was the half-hour change in CO_2 stored below measurement height. Because of the short vegetation (~30 cm), we calculated the change in CO_2 storage by taking the difference in successive CO_2 measurements at the measurement height (Hollinger *et al.* 1994). We used the meteorological convention that positive NEE represents a transfer of CO_2 from the ecosystem to the atmosphere.

Environmental Measurements

Standard meteorological data were collected on a tower adjacent to the EC tower, including photosynthetic photon flux density (PPFD; Li-190SA, Li-Cor Inc. Lincoln, NB.), incident radiation (Li-200SA, Li-Cor Inc. Lincoln, NB), net radiation (REBS Q*7.1, REBS. Inc., Seattle, WA.), relative humidity and air temperature (Vaisala HMP45c, Campbell Scientific Inc., Logan, UT), and wind speed and direction (RM Young 3001, Campbell Scientific Inc., Logan, UT). Soil temperature profiles (5, 10, 15, 20 and 25 cm from surface) were measured with constantan-copper thermocouples and a thermistor (at 5 cm depth only; 107, Campbell Scientific, Logan, UT). Moisture integrated over the top ~15cm of soil was measured with a Campbell CS615 water content reflectometer. All measurements were recorded at half hour average intervals with a CR5000 data logger (Campbell Scientific, Logan, UT). A complete replicate set of micrometerological measurements were collected at a tower 100 m to the NW of EC tower, and were used to interpolate gaps in micrometeorological data measured at the EC tower.

Landscape Properties

To quantify the amount and distribution of land surface subsidence associated with permafrost thaw, a digital elevation model (DEM) was created from point measurements of elevation. Fine scale differences in elevation were measured with a high-resolution differential global position system (dGPS). One GPS unit (Trimble 5400) was placed at a nearby USGS geodetic marker (WGS84, 63°53’16.56”N, 149°14’17.92”W), which acted as the reference

receiver. Using a second GPS unit (Trimble 5400) secured to a backpack, a kinematic survey was conducted by walking transects within a 400 m diameter circle encompassing the EC tower footprint. Geographic position and elevation were collected at 5 s intervals, yielding a total of 7,220 points. These data were post processed with methodology developed by UNAVCO using Trimble Geomatics Office (Dayton, Ohio).

To create the DEM of the area surrounding the EC tower, spherical models were fit to empirical semivariograms, and ordinary kriging was used to interpolate between point measurements using the calculated range of 282 m, a nugget of 0.02, and a partial sill of 0.47. Variogram analysis and kriging was done with the Geostatistical analyst extension in ArcGIS 9.3. Because the study site is on a gentle slope (~5%), the original DEM was corrected for overall slope elevation changes, so we could decipher small-scale subsidence features. To correct for the slope, the DEM was first rescaled so the minimum elevation equaled zero. Mean elevation within 30 m blocks was subtracted from the rescaled DEM, resulting in the deviation in elevation away from the mean plane. This created a map of small-scale variations in topography that we define here as microtopography. Pixel resampling and calculations were done using the aggregate function, resample tool, and the raster calculator in the Spatial Analyst extension in ArcGIS 9.3.

To obtain landscape information in a form comparable to EC data, we extracted information on microtopography corresponding to each wind direction sampled by the EC tower. Virtual transects 200 m in length, originating at the EC tower and radiating out in every wind direction (0-359), were created. A distance of 200 m was chosen because it corresponded to the distance where on average >80% of scalar fluxes originated based on an analytical footprint model (Kormann & Meixner 2001). Microtopography (i.e., local elevation) was sampled every

meter along each transect using Hawth's Analysis Tools (Beyer 2004) in ArcGIS 9.3. The standard deviation of microtopography, which we refer to as roughness, was calculated for each transect (wind direction). This calculated metric was chosen because it captures the variation in microtopography created by permafrost thaw (both subsided areas and raised embankments). Our metric, roughness, should not be confused with the micrometeorological term roughness length.

To calculate our metric, roughness, corresponding to each (half-hour) flux measurement, we simply calculated the standard deviation of the per-meter values of microtopography along the entire transect corresponding to the measured wind direction. We acknowledge that C fluxes measured over a 30-minute period do not emanate from a one-dimensional transect; instead they come from two-dimensional areas in the landscape. To find the best spatial metric corresponding to the measured C flux, we also calculated roughness for the 3 and 5 adjacent transects of the measured wind direction. We found no change in the relationship between C flux and roughness when using a greater number of transects. Also, in principle, footprint models provide more information than the overall radial scale of the area surrounding the EC tower because they help to pinpoint where in the landscape fluxes are originating (Schmid 1997; Schmid & Lloyd 1998; Kormann & Meixner 2001; Schmid 2002). So, for comparison, we also used estimates of the cumulative probability of fluxes coming from different fetches, calculated by a footprint model, to calculate a weighted standard deviation of roughness. However, we chose to use the simple non-weighted roughness because under certain conditions weighting caused relatively flat areas to the SE to have a higher standard deviation than the most subsided areas to the NW. We believe this discrepancy is due to the mismatch in scale between our one-dimensional transects and the two-dimensional cumulative density function calculated by the footprint model (Kormann & Meixner 2001; Kljun *et al.* 2003).

We explored the relationship between roughness and normalized difference vegetation index (NDVI), and the relationship between microtopograghy and active layer depth (ALD). NDVI was calculated using spectral data from an IKONOS image of the site acquired in June 2008. Mean NDVI was calculated for each of the 360 virtual transects radiating out from the EC tower, and was compared to the roughness of the corresponding transect. ALD was measured at 310 locations stratified at various distances within the potential EC footprint, by measuring the length of a metal probe inserted into the soil until the impenetrable frozen layer was reached. The geographic location of each site was measured and subsequently used to extract corresponding values of elevation from the map of microtopography. We only compared ALD to microtopography because we did not have a continuous surface of ALD; therefore, were unable to extract data for the 360 virtual transects to compare with roughness. Relationships were explored with generalized additive models using the mgcv package in R (Wood 2008; R Development Core Team 2010).

Estimation of Landscape Scale Carbon Exchange

To estimate the carbon balance of an ecosystem, missing values in measured CO_2 flux time series must be gap filled to generate a continuous time series of net ecosystem exchange (NEE). We estimated carbon exchange using two gap filling strategies: 1) a novel gap filling strategy using generalized additive models (GAMs) that are flexible enough to incorporate spatial information; 2) nonlinear (NL) relationships with non-spatial environmental variables.

Although NEE is directly measured by the EC technique, the driving force of the exchange is dependent on environmental conditions. Therefore, we modeled NEE for gap filling during winter, growing season (GS) days, and GS nights separately. The beginning and end of the GS was determined by abrupt changes in net radiation corresponding to snowmelt and widespread snow cover, respectively. Generally, the GS began in early May and ended at the end

of September. Data during the GS were split into day and night by ambient light, so when PPFD was greater than 10 μmol m^{-2} s^{-1} daytime conditions were assumed. During daytime, NEE is the balance between gross primary production (GPP) and ecosystem respiration (R_{eco}). To tease apart their contributions, we modeled R_{eco} during GS days using models fitted with GS night data and calculated GPP as the difference between NEE and R_{eco} (GPP = NEE – R_{eco}). Once soil temperature at 5 cm fell below 0°C, winter conditions were assumed. During these conditions, photosynthesis is not occurring so NEE is equivalent to R_{eco}.

Gap filling strategy 1: generalized additive models

To generate a continuous time series, we gap filled NEE using generalized additive models (GAMs), an extension of generalized linear models where a response is modeled as the additive sum of smoothed covariate functions (Hastie & Tibshirani 1990; Wood 2006). With GAMs, nonlinear effects can be modeled without manually specifying the shape of the relationships, which provided us the flexibility to incorporate roughness along with other explanatory variables into the prediction of NEE (Wood 2006; Zuur *et al.* 2009). To control the shape of functions, we used penalized regression splines, which determine the appropriate degree of smoothness of each smoothing function by generalized cross validation (GCV) and adds a "wiggliness" penalty when estimating the coefficients of each smooth with maximum likelihood (Wood 2006). All GAMs used had the basic form:

$$y_i = \beta_0 + f_1(x_i) + f_2(z_i) + f_3(x_i, z_i) + \varepsilon_i$$

where y_i denotes the response variable (NEE or R_{eco}), β_0 the intercept, and functions $f_1(x_i)$ and $f_2(z_i)$ are smooth functions of explanatory variables x_i and z_i and $f_3(x_i, z_i)$ is a two-dimensional smooth function of their interactions. We used thin plate regression splines as the basis for representing smooths (f_1 and f_2) for single covariates and tensor product smooths (f_3) for

interactions (multiple covariates) because they have been found to perform better when covariates are not on the same scale (Wood 2006). We forced the effective degrees of freedom in each model to count as 1.4 degrees of freedom in the GCV score, which forces the model to be slightly smoother than it might otherwise be, this is an *ad hoc* way to avoiding overfitting (Kim & Gu 2004).

Because eddy covariance data are heteroscedastic (Richardson *et al.* 2008) and there were distinct patterns in the residuals, we fit GAMs using a mixed model framework (GAMM) with a Gaussian error distribution to facilitate the incorporation of an exponential variance structure:

$$\varepsilon_i \sim N(0, \sigma^2 * e^V)$$

where the variance of the residuals σ^2 is multiplied by an exponential function of the fitted values (*V)*. We used all data in a single dummy group as our random effect to facilitate the incorporation of the variance structure into the GAM (Wood 2006; Dormann 2007; Zuur *et al.* 2009). All models were fitted using the mgcv package (Wood 2006) in R (R Development Core Team 2010).

A subset of explanatory variables was selected *a priori* including: PPFD, temperature (air, soil at 5cm, depth-integrated soil temperature down to 25cm), roughness, and day of year (DOY). We suspected there might be complex interactions between explanatory variables, so both direct effects and all possible interactions were compared. Models were selected for each time period (Winter, GS day, GS night) during each year (2008, 2009), by starting with the full model containing all variables and interactions and using a form of automatic backward selection in which the penalization term for each smooth could automatically set the term to zero and remove it from the model as appropriate (Wood 2008). We also took into consideration how removing terms affected: (1) the GCV score (the lower the better); (2) the deviance explained

(the higher the better) and (3) the Akaike Information Criterion (AIC, the lower the better; (Anderson *et al.* 1998, 2001).

Because our GAM models incorporated landscape information, they allowed us to estimate the landscapes carbon balance in two different ways. If we assumed the landscape was one unit (measurements taken from one 'population' of fluxes), then gaps in the time series were filled depending on the measured wind direction at the time of the gap. This resulted in a single time series of carbon exchange for the landscape (GAM 1). Alternately, if we assumed the landscape was a combination of multiple patches (wind directions), all absorbing or releasing C simultaneously, then each wind direction was gap filled separately for the entire time series. This resulted in 360 separate time series, whose predictions were averaged to achieve an estimate of carbon exchange for the entire landscape (GAM 360). This method allowed us to estimate C exchange for the entire heterogeneous landscape and made it possible to compare predictions from landscape patches that differed in roughness. Both methods of prediction were done for each time period during 2008 and 2009.

Gap filling strategy 2: non-linear regressions

For comparison we also gap filled data using a more traditional non-linear (NL) regression approach. During GS days, gaps were filled using parameters obtained by fitting half-hour NEE to PPFD using a non-rectangular hyperbola (Thornley & Johnson 1990):

$$NEE = ((\alpha * PPFD * P_{max})/(\alpha * PPFD + P_{max})) - R$$

where α is the linear portion of the light response curve, PPFD photosynthetally active radiation, P_{max} is the asymptote, and R is the intercept or dark respiration term. To capture changes in phenology, parameters were estimated biweekly or monthly depending on the variation among weeks. We incorporated an exponential variance structure due to the heteroscedacity of the data

and used maximum likelihood to estimate parameters using the bbmle package (Bolker 2010) in R.

We were unable to fit exponential models to winter and GS night data separately, so we gap filled with parameters estimated using both data together. Parameters were estimated using the following equation:

$$R_{eco} = \alpha * e^{\beta * T}$$

where α is the intercept and β is the slope, and T was depth-integrated soil temperature during 2008 and soil temperature measured at 5 cm during 2009. We compared models with various forms of temperature (air, soil at 5 cm, depth-integrated soil) and chose the best model based on AIC. We choose not to model average because the best model's AIC was much lower (> 5 pts) than the alternatives. An exponential variance structure was added and parameters were estimated using generalized non-linear least squares using the nlme package in R (Pinheiro *et al.* 2011).

Model Performance

We compared the coefficient of variation (R^2) and Akaike Information Criterion (AIC, (Anderson *et al.* 1998, 2001) of each GAM and NL model, during each time period. Because of the variation in model types, we calculated the R^2 simply as the correlation between the predicted values from each model and the observed values. To assess the predictive performance of the GAM and NL models, we performed cross validation. Ten percent of the data was randomly removed, models were fitted to the remaining data, and these models were then used to predict responses for the withdrawn ten percent. This process was repeated ten times and the root mean square error (RMSE) was calculated for each model. We then compared RMSE of the GAM and NL models within each time period using a t-test at a statistical significance of $P<0.05$. To calculate comparable values of AIC we used the following equation:

$$AIC = 2 * n * \log(RMSE) + 2 * p$$

where n=number of observations and p=number of parameters (Venables & Ripley 2002).

Results

Landscape Heterogeneity of the EC Footprint

Our map of microtopography captured the spatial pattern of ground subsidence created by permafrost thaw within the EML watershed (Figure 2-1). The largest variation in microtopography was found to the NW of the EC tower, while areas to the E and SE were relatively flat. This spatial distribution of ground subsidence agreed well with patterns visible in high-resolution aerial photographs of the site. In addition, the maximum (0.5 m) and minimum (-0.9 m) deviations away from the mean elevation were consistent with field measurements of the depth of individual subsided features and height of raised embankments created by thaw (data not shown). This pattern was mirrored by our calculated landscape metric roughness. Transects with the highest and lowest roughness corresponded with the winds coming from the N-NW and SW-SE, respectively (Figure 3-1).

In general, the depth of the active layer increased as local elevation decreased (became more subsided) and microtopography explained 51% (adj. R^2=0.51) of the observed variation in active layer depth. The relationship was non-linear, with little variation in active layer depth at sites where elevation was positive or slightly negative, followed by an exponential increase in active layer depth as elevation fell below -0.2 m (Figure 3-2A). Transects with more variation in microtopography (high roughness) were found to have higher mean NDVI than transects with less variation (low roughness), and roughness explained 55% of the variation in mean NDVI (adj. R^2=0.55, edf=6.1). This relationship was also non-linear, with NDVI linearly increasing with roughness, then leveling out and sometimes decreasing as roughness increased above 0.14 (Figure 3-2B).

The magnitude of net ecosystem exchange (NEE) increased as the roughness of the landscape increased (Figure 3-3). During GS days, NEE became more negative (more C uptake) with increasing roughness. More C was released from areas with higher roughness during GS nights, but the trend of increased C emission with increasing roughness decreased in magnitude and then reversed during the winter months (Figure 3-3).

Model Performance

GAM models outperformed the non-spatial NL models for gap filling C exchange. GAM models had a higher or equivalent coefficient of determination (R^2) and higher predictive power (lower AIC) than NL models during every time period in both 2008 and 2009 (Table 3-1). During cross validation, GAM models always had lower mean RMSE, but were only significantly lower (at $p<0.05$) during GS days of 2008 and 2009 (Table 3-1).

Predictions of Ecosystem C Balance

In general, the three gap filling methods (NL, GAM 1, GAM 360) resulted in similar estimates of NEE, GPP and R_{eco} for the time periods June 6 through December 8 2008 (weeks 24-48) and April 24 through October 10 of 2009 (weeks 12-40; Figure 3-4). Weekly estimates of NEE, GPP and R_{eco} generated for both GAM methods closely mirror one another throughout both 2008 and 2009 (Figure 3-4). Although the NL and two GAM methods generated similar final estimates of net ecosystem exchange, there were some notable differences. The two GAM methods estimated a slightly higher uptake of carbon (more negative GPP) than their NL counterpart, 10 - 13 gCm^{-2} more in 2008 and 12 – 19 gCm^{-2} more in 2009. This difference in GPP was spread throughout the growing season, with no single week solely responsible for the difference (Figure 3-4A). Similarly, the two GAM methods estimated a slightly higher release of carbon (R_{eco}) than the NL method, 10 -11 gCm^{-2} more in 2008 and 7 – 13 gCm^{-2} more during 2009. Unlike GPP, however, differences in R_{eco} could be attributed to certain time periods.

During 2008, the major differences between the predictions of the two methods occurred during the early growing season (weeks 21-29) where the NL method predicted lower R_{eco} than either GAM method. During the majority of the GS of 2009 the GAM methods estimated higher R_{eco} than the NL method. The other time of divergence among the methods was during transitions into and out of the growing season. The GAM methods predicted lower R_{eco} than the NL method during transition from GS to winter (weeks 39-40) in 2008 and during the transition from winter to GS (week 15-19) in 2009 (Figure 3-4B).

Predictions of Landscape Heterogeneity of C Flux

Using GAMs, we were also able to predict C exchange for each wind direction. To estimate the C balance for the entire landscape we calculated the mean carbon flux of all wind directions for each 30-min interval throughout 2008 and 2009 (GAM 360). This resulted in an estimate of NEE, GPP and R_{eco} for the landscape on average but also allowed us to compare C fluxes from the wind directions with the minimum and maximum roughness to further understand the influence of permafrost thaw and ground subsidence on C flux.

From June to December 2008, GAM 360 estimated the landscape on average took up 337.1 gCm^{-2} via photosynthesis and released 289.5 gCm^{-2} via respiration, resulting in an ecosystem carbon gain of 47.5 gCm^{-2} (Figure 3-5 and Table 3-2). The direction with the maximum roughness had higher GPP and R_{eco} than the landscape on average, while the direction with the minimum roughness had lower GPP and R_{eco} (Figure 3-5 and Table 3-2). This resulted in the direction with maximum roughness gaining 55% more C than the landscape on average, while the direction with minimum roughness gained 76.4% less C (Table 3-2).

From April to October 2009, the landscape on average took up 498.7 gCm^{-2} via photosynthesis and released 410.3 gCm^{-2} via respiration, resulting in a net gain of 87.8 gCm^{-2} (Figure 3-5 and Table 3-2). Again, the direction with the maximum roughness had higher GPP

and R_{eco} than the landscape on average, while the direction with the minimum roughness had lower GPP and R_{eco} (Figure 3-5 and Table 3-2). This resulted in the direction with maximum roughness gaining 41.4% more C than the landscape on average, while the direction with minimum roughness gained 61.7% less C (Table 3-2).

The amplified increase in GPP with maximum roughness was consistent throughout all weeks of the growing season in both 2008 and 2009 (Figure 3-5A). Unlike GPP, the increase in R_{eco} with roughness was not consistent throughout either year. During the GS of both years, the landscape with maximum roughness had higher R_{eco}, but during the winter this trend reversed and the landscape with min roughness had higher R_{eco} (Figure 3-5B). Even though areas with minimum roughness had higher R_{eco} during winter, the overall carbon emission throughout 2008 and 2009 was still greater from areas with maximum roughness (Table 3-2).

Discussion

Quantifying Spatial Heterogeneity

Microtopography is an easy to obtain, integrative metric of the physical and biological changes occurring as the result of permafrost thaw within the EML watershed because it correlates with variables that drive C cycling. Roughness, our landscape level metric of permafrost thaw, captured the variation in microtopography of each wind direction sampled by the EC tower (Figure 3-1). We found that as microtopography decreased (ground became more subsided), active layer depths (ALD) increased, exponentially increasing after a threshold (Figure 3-2A). This pattern is a result of changes in soil thermal conductivity created by the redistribution of water into subsided areas, which increases soil temperature within depressions while decreasing temperatures in higher, dryer areas (Jorgenson *et al.* 2001; Kane *et al.* 2001; Osterkamp *et al.* 2009). These physical changes in soil moisture and temperature drive variable depths of thaw across the hillslope. This landscape level pattern of ALD and subsidence is

consistent with previous work at this site, which showed similar relationships between microtopography, temperature, and moisture (Vogel *et al.* 2009; Lee *et al.* 2010).

Areas with greater roughness had higher mean NDVI, with NDVI increasing with roughness until a threshold was reached (Figure 3-2B). Unlike ALD, NDVI leveled out and slightly decreased at the upper end of the roughness scale. NDVI has been shown to be positively correlated with leaf area index (Tucker 1979; Williams *et al.* 2008), aboveground biomass (Sellers 1987; Boelman *et al.* 2003), net primary production (Goward *et al.* 1985), GPP and R_{eco} (Boelman *et al.* 2003; Vourlitis *et al.* 2003; La Puma *et al.* 2007). Permafrost thaw within the EML watershed causes a shift in species composition from a plant community dominated by tussock-forming sedges to a community with increased shrub and moss abundance, and concurrently an increase in biomass and productivity (Schuur *et al.* 2007; Vogel *et al.* 2009). Our result of increased NDVI with increased roughness is consistent with this pattern of increased biomass and productivity with thaw and also indicates that an upper limit of productivity may be reached as permafrost thaw continues and plants respond to the changing conditions. This upper limit is likely driven by the size of shrub species currently at the site, but could increase in the future, on the timescale of plant succession, if boreal trees were to increase in abundance at this tundra site.

These relationships between microtopography and important biophysical features of the landscape (ALD & NDVI) highlight the feasibility of using remotely sensed spatial information to improve estimates of regional C balance in high latitude ecosystems. Recent advancements in sensor resolution (e.g. LIDAR) now make microtopographical mapping of these vast, remote areas possible.

Incorporating Spatial Heterogeneity into EC C Estimates

We incorporated the spatial variability of C flux into the EC estimate of C exchange during gap filling using generalized additive models (GAMs). Because a continuous time series is required to estimate C balance, missing time periods must be modeled (Falge *et al.* 2001; Baldocchi 2003). This gap-filling step provided a method for predicting C exchange based on the roughness of the landscape in specific wind directions, as well as more accurately determining the C balance of the entire landscape. We found that GAMs were equivalent or superior to traditional NL regression approaches (Table 3-1). GAMs had higher predictive power and a higher or equivalent coefficient of variation (R^2) than the NL models during all time periods. During cross validation, GAMs consistently had lower RMSE than NL models over all time periods, but were statistically lower only during GS days. The lack of statistical improvement in RMSE during GS nights and winter by the GAMs is not surprising because these time periods are notoriously difficult to model using any procedure (Baldocchi 2003). Overall, our model comparison to the more traditionally used NL gap filling models gave us confidence that adding model complexity to include spatial information was justified.

The aggregated predictions of C exchange from the GAM and NL models did not substantially differ from one another throughout either 2008 or 2009 (Figure 3-4). However, there were notable time periods where the two methods diverged in their predictive capabilities. During the early growing season of 2008 (weeks 21-29), the GAM substantially over-predicted R_{eco} compared to the NL model (Figure 3-4B). We believe this difference is due to a lack of data during the early GS, which caused the GAM to miss the upswing of R_{eco} that coincides with rapid changes in phenology during the spring. Predictions of R_{eco} and NEE from the NL and GAM also diverged during the transition from the GS to winter in 2008, and the transition from the winter to the GS of 2009 (Figure 3-4B & Figure 3-4C). We attributed this sensitivity to

seasonal transitions by the GAM to the flexibility of their smoothing functions, which can capture rapidly changing trends in the data (Zuur *et al.* 2009). Because the NL models' empirically derived parameter estimates depend on relationships that change dramatically in this highly seasonal ecosystem, the relationships would need to be continuously updated in order to capture these transitions (Falge *et al.* 2001; Baldocchi 2003). Biologically, the dip in R_{eco} during the transition in and out of winter could be attributed to changes in microbial species composition, or to the disruption of biological activity by the state change (freezing-point) of water (Rivkina *et al.* 2000; Mikan *et al.* 2002). This dip in R_{eco} could also be caused by shifts in the availability and use of substrates by microbes between the GS and winter (Hobbie *et al.* 2000; Dioumaeva *et al.* 2003; Davidson & Janssens 2006).

Effects of Spatial Heterogeneity on C Flux

By incorporating spatial information, we were able to estimate the C balance of the landscape in two different ways. First, we filled gaps depending on the measured wind direction at the time of the gap and created a single time series of C exchange for the entire landscape (GAM 1). Second, we gap filled the entire time series for each wind direction separately and averaged the predictions to estimate the C balance of the landscape (GAM 360). This allowed us to estimate C exchange for the entire heterogeneous landscape and also make predictions for the wind directions with the minimum and maximum roughness. Final C estimates from GAM 1 and GAM 360 were nearly identical (Figure 3-4). This similarity indicates that the wind distribution sampled by the EC tower was sufficient to capture the variability of thaw seen across the entire radial landscape surrounding the tower.

The landscape on average (GAM 360) was a C sink during both 6-month measurement campaigns. The wind direction with the most variation in microtopography (maximum roughness), resulting from permafrost thaw and ground subsidence, had both higher GPP and

R_{eco} than the landscape on average (Figure 3-5A & Figure 3-5B), while the wind direction with least variation (minimum roughness) exhibited lower GPP and lower R_{eco}. Overall, during the 6-month campaign of 2008, the area with highest roughness gained 55.2% more C than the landscape on average, while the area with lowest roughness gained 76.4% less C. Similarly, during the 6-month campaign of 2009, the area with the highest roughness gained 41.4% more C, while the areas with lowest roughness gained 61.7% less C (Table 3-2). Based on these results, permafrost thaw and ground subsidence amplifies both GPP and R_{eco}.

The amplification of GPP with roughness was consistent throughout the GS of both 2008 and 2009 (Figure 3-5A & Figure 3-3). This enhanced C sequestration could be due to shifts in the plant community to more highly productive species as permafrost thaws(Schuur *et al.* 2007; Osterkamp *et al.* 2009), or to increased plant productivity due to greater nutrient availability resulting from enhanced decomposition within subsided areas (Shaver *et al.* 1992; Mack *et al.* 2004; Vogel *et al.* 2009; Natali *et al.* in review). Our results of higher NDVI in areas with higher roughness also support the idea of increased productivity as permafrost thaws (Figure 3-2B), as do several other studies that show NDVI is positively correlated with both R_{eco} and GPP (Boelman *et al.* 2003; Vourlitis *et al.* 2003; La Puma *et al.* 2007).

Ecosystem respiration also increased in areas of the landscape with greater roughness during the GS of both years (Figure 3-5B & Figure 3-3), likely because of greater temperature and moisture associated with greater ALD (Figure 3-2A; (Vogel *et al.* 2009; Lee *et al.* 2010)). More organic C is exposed to above freezing temperatures as ALD increases. These abiotic changes stimulate decomposition and nitrogen mineralization, which result in increased heterotrophic respiration (Shaver *et al.* 1992). Vogel et al (2009) found that as subsidence increased, ALD increased and, in conjunction, both GPP and R_{eco} increased. These results are

consistent with a large body of work showing that temperature and moisture are often the major determinates of organic matter decomposition and ecosystem respiration (Oberbauer *et al.* 1991; Shaver *et al.* 1992; Hobbie *et al.* 2000; Xu & Qi 2001; Davidson *et al.* 2002; Davidson & Janssens 2006). There is also increased autotrophic respiration from more highly productive plants in subsided areas contributing to the overall increase in R_{eco} during the GS (Schuur *et al.* 2007; Vogel *et al.* 2009).

In contrast to the GS, areas with increased roughness had lower C emissions during the winter (Figure 3-5B & Figure 3-3). Even though areas with less roughness had higher R_{eco} during winter, the overall C emission throughout 2008 and 2009 was still greater from areas with highest roughness. The reversal of the relationship of roughness and R_{eco} during the winter is opposite previous work at the site that estimated more subsided areas have greater C emissions (Vogel *et al.* 2009). They attributed greater winter C flux from subsided areas to warmer soils resulting from delayed active layer refreezing and the added insulation from snow accumulating in subsided areas, but data in the critical winter months was admittedly scarce (Hinkel & Hurd 2006; Vogel *et al.* 2009). The inconsistency of our data may be due to differential diffusion through variations in snow cover trapped in subsided areas. The coefficient of variation of the top GAM was also very low, only 0.16 and 0.22 during winter of 2008 and 2009, respectively. Overall, there was little variation in winter C flux (throughout space or time) and we believe more measurements are needed before our winter pattern can be fully supported. More winter data is also crucial for determining the ecosystem's annual C balance and its feedback to climate change.

Concluding Remarks

We estimated the C balance of a heterogeneous landscape undergoing permafrost thaw by incorporating spatial variation into an eddy covariance estimate. We found strong relationships

between thaw induced ground subsidence and ALD and NDVI, which both correlate with C flux. These microtopographical changes also strongly correlated with NEE. By using GAMs, we incorporated these spatial relationships back into final EC C balance estimates during gap filling. Thus, we achieved a more accurate C estimate for the heterogeneous landscape and could make predictions for areas undergoing various degrees of permafrost thaw. Using GAMs, we were better able to predict C exchange during seasonal transitions, which indicates this type of gap filling strategy would be good in systems with high temporal variability. Because all natural ecosystems vary through space and time, we believe GAMs can be an important tool for achieving more accurate C estimates. The use of GAM's will also allow EC towers to be placed in more heterogeneous environments than they have been previously used.

As permafrost thaws within this upland tundra ecosystem, a heterogeneous environment is created by changes in microtopography. We found this ecosystem was a C sink during two consecutive years, and areas with greater thaw exhibited greater C sequestration (GPP) and greater C loss (R_{eco}). Thawing of permafrost increases the amplitude of the C cycle, which has important implications for the future landscape-level C balance (Zimov *et al.* 1996). Currently, GPP is stimulated more than R_{eco}, but this balance may shift because we found that NDVI diminished with increased permafrost thaw indicating there may be an upper limit in productivity, unless successional changes in vegetation occur.

Although we found the ecosystem was a C sink during the measurement campaigns of both years, this is not representative of the annual C balance. We did not measure C flux during a portion of the winter season, and even though C fluxes during this time period are relatively low, the length of the season make it very important. By linearly extrapolating between these missing

winter periods, we found that annually the ecosystem became a C source of 60 $gCm^{-2}year^{-1}$ and 13 $gCm^{-2}year^{-1}$ in 2008 and 2009, respectively.

Table 3-1. Coefficient of variation (R^2), predictive power (Δ AIC) and cross validation root mean square error (RMSE ± standard deviation) for GAM and NL models during GS day (GS-D), GS nights (GS-N), and winter of 2008 and 2009.

Time Period	Model	R^2	Δ AIC	RMSE
GS-D 2008	GAM	0.83	0	0.067±0.03*
	NL	0.78	2458.6	0.161±0.06
GS-N 2008	GAM	0.26	0	0.132±0.09
	NL	0.26	93.4	0.151±0.10
Winter 2008	GAM	0.16	0	0.047±0.04
	NL	0.01	116.9	0.053±0.05
GS-D 2009	GAM	0.83	0	0.052±0.02*
	NL	0.78	5971.8	0.181±0.17
GS-N 2009	GAM	0.29	0	0.085±0.06
	NL	0.22	772.9	0.136±0.09
Winter 2009	GAM	0.22	0	0.041±0.03
	NL	0.12	363.7	0.065±0.06

* Significantly different than model counterpart at $p<0.05$

Table 3-2. Carbon estimates (GPP, R_{eco}, NEE) in g C m^{-2} for the wind direction with the minimum roughness (Min), maximum roughness (Max) and the average (Avg) of all 360 wind directions during June to December 2008 and April to October 2009. Negative numbers denote when the ecosystem is taking up carbon.

	2008			2009		
Roughness	GPP	R_{eco}	NEE	GPP	R_{eco}	NEE
Min	-300.3	288.3	-11.2	-403.6	386.6	-33.6
Max	-397.4	291.9	-106.1	-586.4	450.6	-149.8
Avg	-337.1	289.5	-47.5	-498.7	410.3	-87.8

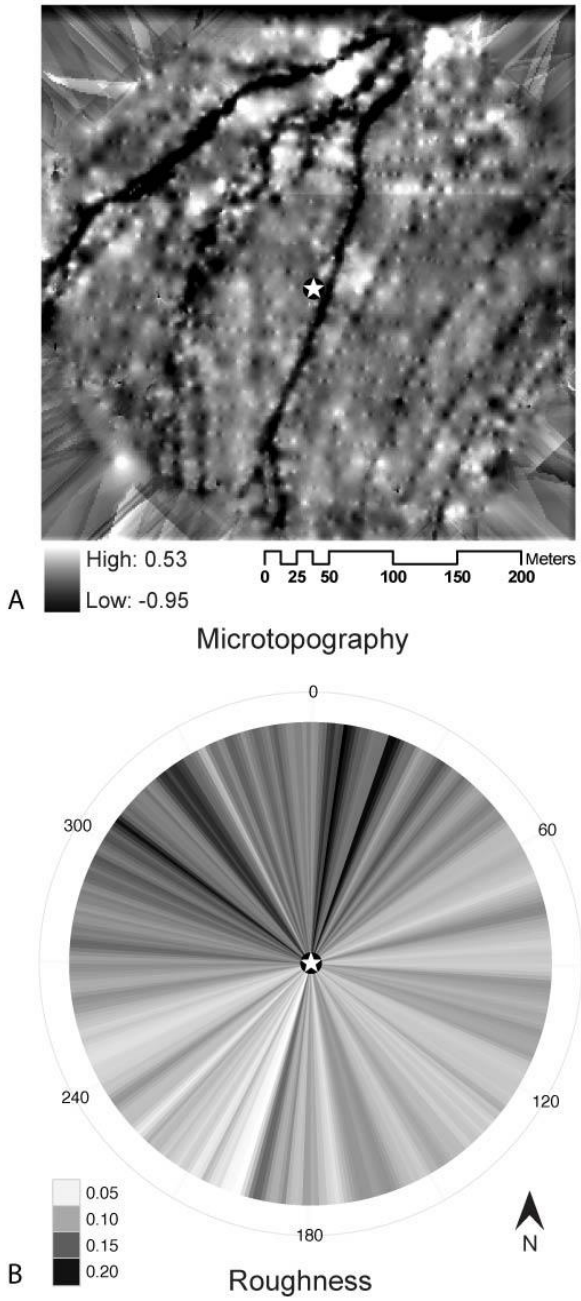

Figure 3-1. Map of microtopography and 360 transects surrounding the EC tower. A) Map of microtopography surrounding the EC tower (✪), with lighter shades indicating areas where the ground surface is higher than the mean elevation of the landscape, and darker shades where the ground surface was lower than the mean elevation (i.e. subsided). B) 360 transects radiating out from EC tower (✪) corresponding to the wind direction sample by the tower. The color of transects grades from white to black as the degree of roughness increases. Note that in general the roughest transects occur to the North and North West of the EC tower, while transects to the South and East have lower roughness.

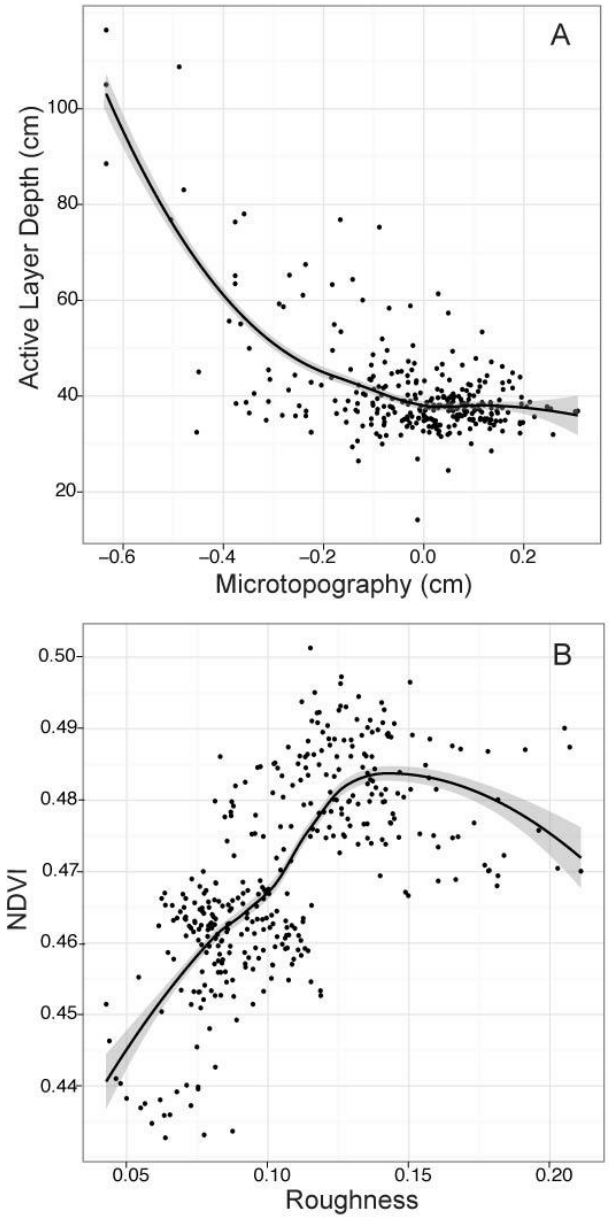

Figure 3-2. Relationships between microtopography and ecosystem properties. A) Non-linear relationship between active layer depth (ALD; cm) and microtopography (adj. R^2=0.51) with 95% confidence intervals. Note the small amount of variation in ALD where microtopography is positive or slightly negative, then an exponential increase in ALD as microtopography falls below -0.2 m. B) The non-linear relationship between mean NDVI and roughness (adj. R^2=0.55) with 95% confidence intervals. NDVI linearly increases until roughness reaches 0.14, then NDVI levels out or decreases.

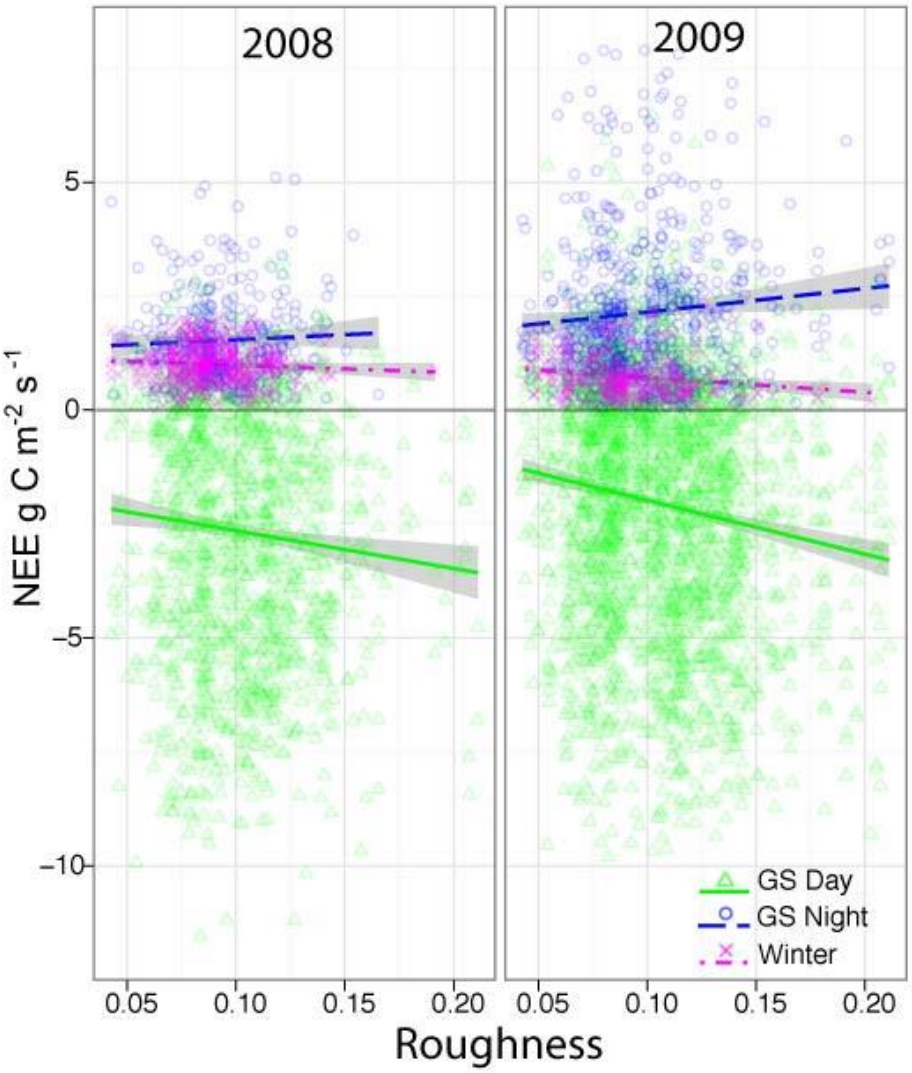

Figure 3-3. Relationships between roughness and net ecosystem exchange (gC m^{-2}) during GS nights, GS day and winter. Actual data points displayed behind the trend lines.

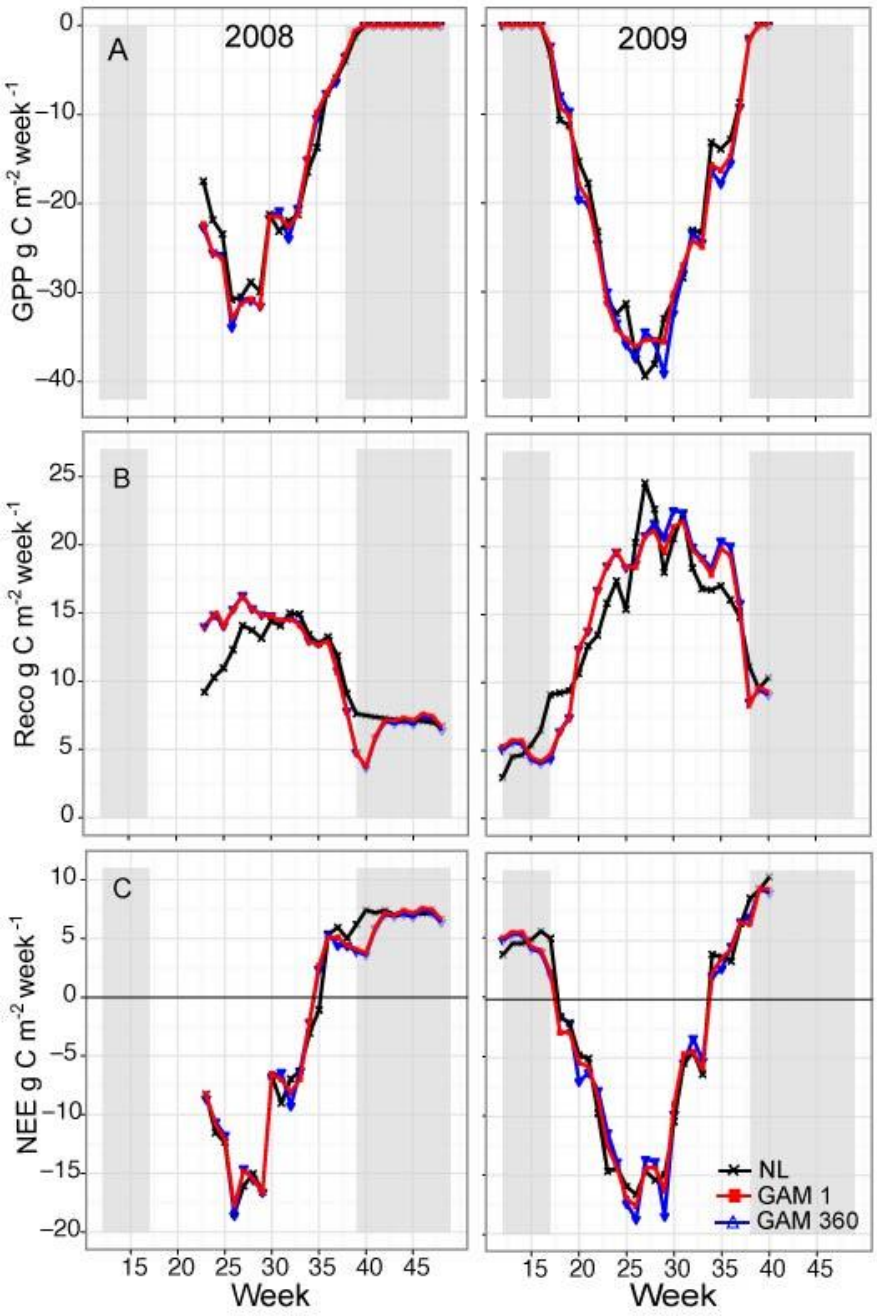

Figure 3-4. Carbon fluxes for the three methods of prediction. A) Gross primary production (GPP: gCm^{-2}), B) ecosystem respiration (R_{eco}: gCm^{-2}), and C) net ecosystem exchange (NEE: gCm^{-2}) for the three methods of prediction: GAM 360, GAM 1 and NL over the measurement campaigns of 2008 and 2009. Shaded areas denote winter conditions and negative values occur when the ecosystem is a C sink.

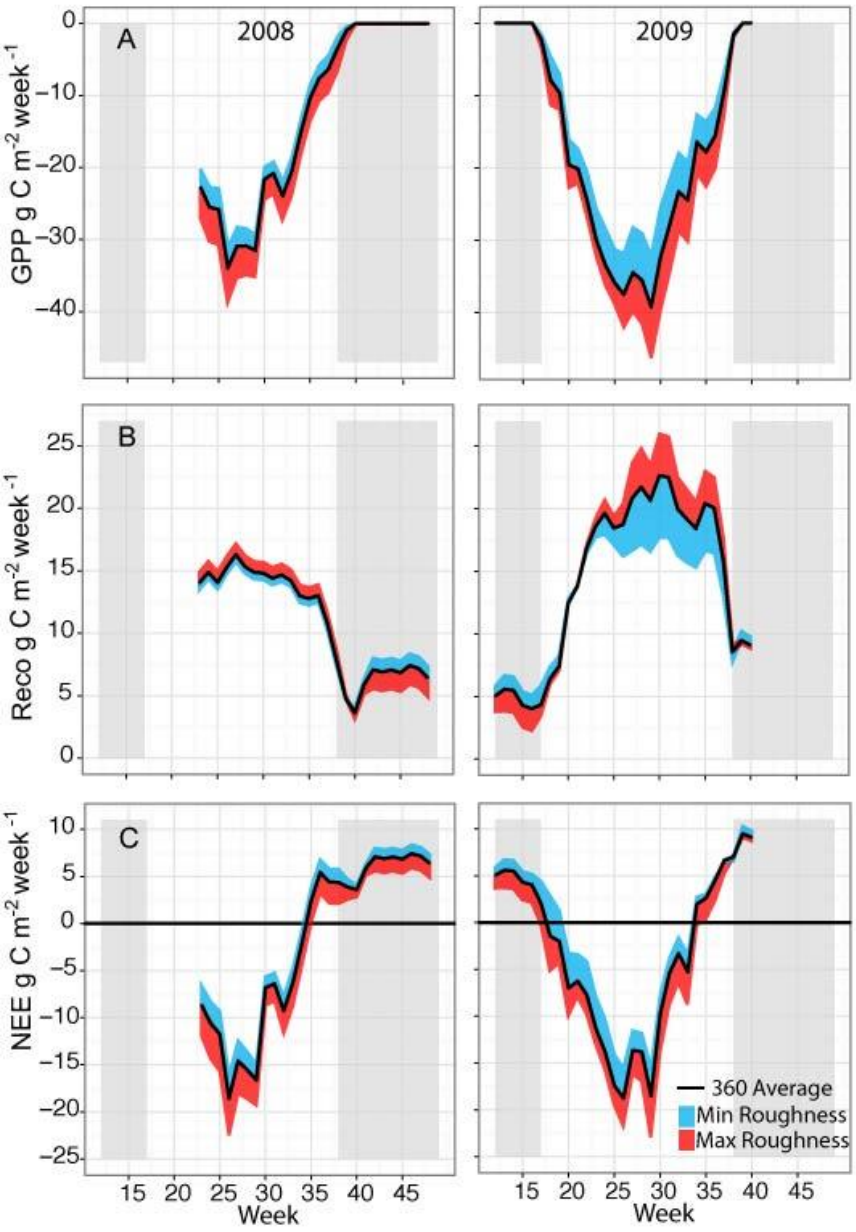

Figure 3-5. Carbon fluxes for different wind directions. A) Gross primary production (GPP: gCm^{-2}), B) ecosystem respiration (R_{eco}: gCm^{-2}), and C) net ecosystem exchange (NEE: gCm^{-2}) for the landscape on average (360 Average) and for the wind direction with max roughness and min roughness over the measurement campaigns of 2008 and 2009. Shaded areas denote winter conditions and negative values occur when the ecosystem is a sink.

CHAPTER 4
TUNDRA ECOSYSTEMS OBSERVED TO BE CO2 SOURCES DUE TO DIFFERENTIAL AMPLIFICATION OF THE CARBON CYCLE

Background

Over the past five decades, researchers have tried to determine whether high latitude ecosystems will become a source of carbon (C) to the atmosphere, or remain a sink, as climate changes. This question is of global importance because these ecosystems cover large areas of the northern high latitudes and store vast quantities of organic C in their soils (Schuur *et al.* 2008; Tarnocai *et al.* 2009). Based on their large standing stocks of carbon, researchers have determined that these ecosystems have been, on average, a C sink for the past 10,000 years (Harden *et al.* 1992; Hicks Pries *et al.* 2012). The ability of tundra to sequester and store carbon is due to long, harsh winters and poorly drained permafrost soils, which create conditions that slow decomposition relative to plant production (Chapin *et al.* 1980; Miller *et al.* 1983; Billings 1987; Post 1990; Oechel & Billings 1992; Hobbie *et al.* 2000). But temperatures in high latitudes are rising (Chapin *et al.* 2005; IPCC 2007). The response of the carbon cycle to this climate forcing is of vital importance but the magnitude and timeline of change is uncertain.

Two opposing feedbacks within the carbon cycle will determine the future C balance of tundra ecosystems. Rising temperatures resulting from increased atmospheric CO_2 concentrations could warm and thaw permafrost soils and stimulate decomposition and ecosystem respiration, resulting in a positive feedback to climate change by further increasing atmospheric CO_2 concentration (Shaver *et al.* 1992; Hobbie *et al.* 2002; Schuur *et al.* 2008; McGuire *et al.* 2009; Grosse *et al.* 2011). On the other hand, increases in temperature and CO_2 concentration could stimulate primary production. Stimulation effects could be direct through effects on plant

---

Belshe EF, EAG Schuur, BM Bolker (submitted) Tundra ecosystems observed to be CO_2 sources due to differential amplification of the carbon cycle. Ecology Letters.

physiology, or indirect through increases in plant-available nutrients released from decomposing organic matter and/or lengthening of the growing season (Shaver *et al.* 1992; Johnson *et al.* 2000). If gross primary production exceeds ecosystem respiration, the ecosystem will sequester CO_2 from the atmosphere and act as a negative feedback to climate change.

Much effort has gone into quantifying the carbon balance of tundra ecosystems and understanding the controls over carbon uptake and emission. Previous studies of growing season CO_2 exchange have shown initial release of CO_2 in the 1980s (Oechel *et al.* 1993), followed by a longer-term response of increased growing season CO_2 uptake (Oechel *et al.* 2000; Ueyama *et al.* in press). However, growing season patterns of CO_2 flux are only a part of the picture and by themselves do not provide complete information about the trajectory of tundra ecosystems. Winter CO_2 emissions have been recognized as an integral part of tundra carbon balance, and although there is considerably less winter data in the literature, recent efforts have improved our knowledge of the controls over winter CO_2 flux (Fahnestock *et al.* 1998; Fahnestock *et al.* 1999; Welker *et al.* 2000; Grogan & Jonasson 2006; Nobrega & Grogan 2007; Sullivan *et al.* 2008; Rogers *et al.* 2011). However, a regional synthesis of winter CO_2 emission is missing.

In this meta-analysis we compiled CO_2 flux observations from both growing season and winter time periods. Using time-series analysis, we assess whether seasonal or annual CO_2 fluxes have changed over time. By comparing CO_2 fluxes from different sites, we investigated the response of the carbon cycle to local differences in climate. Our intent is to revisit the question of whether tundra ecosystems are sources or sinks of CO_2, and to determine if we have observational evidence to support either trajectory.

Material and Methods

Literature Search

We compiled published observational data on CO_2 flux (Gross Primary Production: GPP, Ecosystem Respiration: ER, Net Ecosystem Exchange: NEE) from fifty-four studies at 32 different sites (Figure 4-1) (Johnson 1970; Coyne 1975; Poole 1982; Grulke *et al.* 1990; Giblin *et al.* 1991; Oechel *et al.* 1993; Oechel *et al.* 1995; Oberbauer *et al.* 1996; Oechel *et al.* 1997; Vourlitis & Oechel 1997; Fahnestock *et al.* 1998; Hobbie 1998; Oberbauer *et al.* 1998; Oechel *et al.* 1998; Fahnestock *et al.* 1999; Grogan & Chapin 1999; Jones *et al.* 1999; Vourlitis & Oechel 1999; Welker *et al.* 1999; Oechel *et al.* 2000; Soegaard *et al.* 2000; Vourlitis *et al.* 2000a; Vourlitis *et al.* 2000b; Welker *et al.* 2000; Zamolodchikov *et al.* 2000; Heikkinen *et al.* 2002; Harazono *et al.* 2003; Epstein *et al.* 2004; Heikkinen *et al.* 2004; Grogan & Jonasson 2006; Kwon *et al.* 2006; Groendahl *et al.* 2007; Kutzbach *et al.* 2007; Lafleur & Humphreys 2007; Nobrega & Grogan 2007; van der Molen *et al.* 2007; Arens *et al.* 2008; Nobrega & Grogan 2008; Sjögersten *et al.* 2008; Sullivan *et al.* 2008; Vogel *et al.* 2009; Huemmrich *et al.* 2010; Taggeson *et al.* 2010; Zona *et al.* 2010; Humphreys & Lafleur 2011; Olivas *et al.* 2011; Rocha & Shaver 2011; Rogers *et al.* 2011; Belshe *et al.* 2012; Euskirchen *et al.* 2012; Trucco *et al.* 2012; Ueyama *et al.* in press; Natali *et al.* in review). NEE is the net exchange of CO_2 between the atmosphere and the ecosystem over a time interval (Baldocchi 2003) and is the balance of two strong, opposing processes during the growing season: CO_2 uptake by primary producers (gross primary production, GPP) and respiration losses of CO_2 by both primary producers and heterotrophs (ecosystem respiration, ER). During winter, tundra vegetation is covered by snow and photosynthesis is negligible, therefore NEE is effectively equivalent to ER. We used the convention that negative values indicate CO_2 uptake by the ecosystem (Baldocchi 2003).

We gathered CO_2 flux data by conducting an Internet survey of ISI Web of Science and Google Scholar using keywords 'carbon AND tundra'. We only included studies containing CO_2 flux observations from tundra ecosystems. As a second line of investigation, we contacted all lead investigators identified during our initial literature search and inquired about any additional studies that were previously overlooked. As a second filter for our meta-analysis, we only included studies if flux measurements were distributed throughout the season (growing season or winter) and spanned the range of conditions encountered at each site. As a third filter, we only included studies from sites with 'tundra' vegetation, although we recognize that this category includes a variety of plant communities across a moisture gradient. We specifically excluded studies from high latitude forests, as well as fens, bogs, and mires, because these wetlands have different controls over carbon balance. We were interested in non-manipulated fluxes but also report control or ambient CO_2 flux estimates from experimental manipulations. For comparison, all data are reported as total seasonal fluxes in g C m^{-2} for either growing season or winter time periods. Because there was a wide range in the interpretation of what constitutes the growing season and winter, and to follow conventions comparable with previous meta-analyses (Oechel *et al.* 1993; Oechel *et al.* 2000), we standardized the length of the growing season (100 days) and winter (245 days) by dividing seasonal estimates by the length of the reported season to estimate average daily (g C m^{-2} d^{-1}) flux. We then multiplied daily estimates by the standardized growing season and winter length. We chose season lengths based on the average length of the seasons reported in our meta-analysis, which is why the length of the growing season (100 days) and winter (245 days) does not add up to a full year. During the remaining 20 days, at the season transitions, CO_2 fluxes are roughly balanced with GPP=ER (i.e. net flux is approximately zero), so excluding these periods does not alter estimates of annual flux derived by adding growing

season and winter estimates. Data were gathered on climate corresponding to the year when CO_2 fluxes were measured (mean annual temperature: MAT, total annual precipitation: TAP) for each of the 32 sites sampled (Figure 4-1) from the University of Delaware precipitation and air temperature data set on NOAA/OAR/ESRL PSD, Boulder, Colorado, USA, at http://www.esrl.noaa.gov/psd/. These weather data are a gridded interpolation of land station data and have a spatial resolution of 0.5 x 0.5 degrees, which may reduce data variation of near-by sites. If data were reported as an average of multiple sites, we report the average climate conditions.

Data Analysis

To elucidate changes in the tundra carbon cycle over space and time, we explored both temporal trends in CO_2 fluxes and relationships among CO_2 fluxes and spatial differences in climate. First, we examined how seasonal CO_2 fluxes have changed over the last four decades, and estimated the historical annual CO_2 balance from our temporal estimates. Temporal trends in growing season and winter CO_2 fluxes were estimated using a linear mixed effect model with site and site x year interaction as random effects to account for variation in the slopes with respect to time due to local site differences. There was a small but significant correlation between year and long-term average (1950-2000) temperature ($r=0.21$; $p=0.003$), and long-term average precipitation ($r=0.32$; $p=0.001$) for sites included in the analysis. An autoregressive (AR1) correlation structure was added to the model to account for temporal autocorrelation within sites. Flux estimates were aggregated by site for each year and weighted by the number of observations within each site-year combination. Simulations of the null hypothesis (no overall trend at the population level) suggested that this approach was anticonservative, with a type-I error rate of approximately 0.1 for a nominal p-value of 0.05; therefore, we used parametric bootstrapping to achieve an appropriately conservative estimate for the significance of the trend

(Booth 1995). Because our winter data were insufficient to support such a complex analysis, we did not include the correlation structure in the winter model and only included site (not the site x year interaction) as a random effect. To calculate an annual estimate of tundra CO_2 balance, we fitted the growing season model to a restricted data set containing only sites sampled during winter (to avoid calculating an annual estimate from disparate sites). We then summed the predicted values from the restricted growing season and winter models to calculate the annual estimate. The variance of the annual estimate was estimated as the sum of the variances of the winter and growing season models (Lyons 1991).We used a Student's t-test of the differences in estimated slopes in order to determine significant seasonal differences in the rates of change through time.

Second, we used simple linear regressions to explore if the observed variation in CO_2 fluxes (NEE, GPP, ER) during the growing season and winter were related to spatial differences in climate (MAT & TAP). Because MAT and TAP were highly correlated ($r=0.7$; $p<0.001$) for sites in our analysis, and the observational record of temperature is much stronger, we present only results from MAT, recognizing that responses to temperature and precipitation are strongly confounded. We also explored the use of growing season (June-Aug.) temperature to explain growing season trends in CO_2 fluxes, but found MAT explained more overall variation (higher adjusted R^2). In addition, slopes estimated with growing season temperature did not differ from MAT estimated slopes for either GPP or ER, and growing season temperature was a non-significant predictor of growing season NEE ($p=0.47$); therefore, we use MAT in our analysis of both seasons. To determine if the growing season or the winter was responding more strongly to changes in MAT, we tested for the difference between slopes using a Student's t-test. Similar to the temporal analysis above, we calculated an annual response to temperature by adding

estimated growing season and winter trends together. All models were fit using the base and nlme packages, version 3.1-98 (Pinheiro *et al.* 2011), and graphics were produced using ggplot, version 0.8.9 (Wickham 2009) in R (R Core Development Team 2011).

Results

Changes in CO_2 Flux Over Time

Over the past four decades, tundra ecosystems measured during the growing season have been found to be both CO_2 sources and CO_2 sinks, but overall growing season NEE has been decreasing over time (i.e., net CO_2 uptake is increasing: Figure 4-2). Seventy percent of the total growing season NEE observations were below zero (net CO_2 uptake). Across the full dataset, growing season NEE has decreased -3.8±1.4 g C m^{-2} yr^{-1} (standard *F* test p=0.007; bootstrap adjusted p=0.03). Due to the limited number of sites and sparse observations at individual sites during the 1980s, we repeated this linear analysis using data collected post-1990, when the majority of observations were collected. The decreasing trend of growing season NEE for this period is -4.5±0.9 g C m^{-2} yr^{-1} (bootstrap adjusted p= 0.005), which amounts to an estimated cumulative increase of 90 g C m^{-2} of net growing season C uptake between 1990 and 2010. Before 1990, the limited number of sites and sparse observations do not allow for robust tests of trends through time; thus the best-fit line extending through the whole dataset is not well constrained for the early decades of the dataset.

The trend in winter CO_2 emissions over time (1.5±1.1 g C m^{-2} yr^{-1}), across the entire winter dataset (1979-2010) was much weaker and not statistically significantly different from zero (Figure 4-2B; p =0.18), when including a random intercept to control for among-site differences. However, the winter CO_2 flux dataset overall has many fewer sites, and fluxes at individual sites are more sparsely quantified in comparison to growing season studies. Early records in the winter dataset came from relatively cold sites only. The middle period (1995 -

2000) contains a wider range of sites, but come mostly from sites sampled only during one year. The most recent period of the record (from 2004 to 2010) contains sites that span the range of environmental conditions (MAT, MAP), and includes multiple sites monitored over several seasons that have more coherent with-site trends. In the latest period alone, we find a significant increase in winter CO_2 emissions over time, with an estimated increase of 15.9±4.3 g C m-2 yr^{-1} (p=0.002;Figure 4-2B). This increase in recent CO_2 emissions could be due to a recent amplification of winter CO_2 emissions or to the stronger data record, which improved our ability to estimate temporal trends in winter CO_2 flux. However, the exact slope of the line may not be representative of longer-term trends because it is fit to only seven years of data.

Estimates of annual CO_2 flux based on combining growing season and winter regressions show that the mean flux across the dataset ranged from an estimated net loss of 82 g C m^{-2} yr^{-1} in 1979 to an estimated loss of 21 g C m^{-2} yr^{-1} in 2010 (Figure 4-3). In the early 1980s it was not possible to determine if this net loss was statistically different from C neutral due to data scarcity. But for several decades from the mid 1980s until the early 2000s tundra ecosystems were a net source of CO_2 to the atmosphere, with a mean net loss of 76 g C m^{-2} yr^{-1} in 1982 and a net loss of 36 g C m^{-2} yr^{-1} in 2002. By the mid 2000s, the overall declining but statistically insignificant annual trend (est=-2.0±1.9; p=0.18) pushed the estimated annual CO_2 flux towards net C neutrality. Clearly, observed increases in growing season CO_2 uptake are shifting tundra sites toward becoming a CO_2 sink on an annual basis. But the magnitude of the more uncertain winter emissions also plays a role. Using the winter trend from the recent data intensive period (2004-2010;Figure 4-3B) counterbalances the shift toward C neutrality and reverses the trend through time, resulting in a continued increase in CO_2 emissions on an annual basis (Figure 4-3B). Although it is hard to know how trends documented over a 7-year period will change in the

future, this highlights the important role of winter CO_2 emissions in determining annual CO_2 exchange, and emphasizes the need for more sustained winter CO_2 flux data from a variety of locations.

Relationships Between CO_2 Flux and Spatial Differences in Climate

To identify potential factors driving temporal trends in CO_2 flux, we explored patterns among CO_2 fluxes and spatial differences in MAT. We recognize that MAT is highly correlated with precipitation at the sites included in our analysis, so we are using MAT as a proxy for the general climate influence on CO_2 flux. Both growing season CO_2 emissions (Figure 4-4A) and CO_2 uptake (Figure 4-4B) are greater at sites with higher temperatures, with an overall negative trend between MAT and growing season NEE. This corresponds to higher net growing season CO_2 uptake at sites with higher MAT (Figure 4-4C). The slope of the growing season GPP trend is significantly greater than the slope of the growing season ER trend (est=-3.6±2.0; p =0.05), suggesting that growing season GPP responds more strongly than growing season ER to differences in MAT. In addition, the analysis of growing season CO_2 flux by MAT, in contrast to the analysis with time, does not feature positive growing season CO_2 fluxes where CO_2 losses from respiration would need to be greater than plant uptake. This suggests that the period of net CO_2 loss predicted by the regression model before 1990 (Figure 4-2) was actually driven by data scarcity and influential points measured early in the record.

During the winter, when only heterotrophic respiration is occurring, sites with higher MAT exhibited greater CO_2 emissions (Figure 4-4D). The estimate of predicted net annual (winter plus growing season) CO_2 flux is positive throughout the range of temperatures (Figure 4-5), yet there was no statistical difference between the absolute value of slopes of the growing season and winter trends (est.=1.9±2.0; p=0.2). This suggests that both growing season and winter CO_2 flux have similar responses to changes in MAT, but the magnitude of the CO_2

emission exceeds the temperature response of CO_2 uptake. Based on predictions from the annual response, mean annual C emissions should range from 23 to 56 g C m^{-2} across the gradient of tundra temperatures, and a 1°C increase in temperature would increase annual emissions by 2 g C m^{-2}. These results indicate that the recent amplification of arctic temperature should have increased both CO_2 uptake and CO_2 emission at a similar rate, but that ultimately the source strength of tundra ecosystems is greater on an annual basis.

Discussion

In spite of the spatial variation in climate, soil characteristics, vegetation composition, and site histories within the tundra biome (Callaghan *et al.* 2004), our meta-analysis detected an apparent regional amplification of the C cycle in recent decades. Growing season net CO_2 uptake has definitively increased since the 1990s, and trends point towards a potential increase in winter CO_2 emissions, especially in the last decade (Figure 4-3). Changing temperature, and the factors that covary with it, may have played a role in this amplification and based on the relationship with site mean annual temperature (Figure 4-5), CO_2 emissions exceed CO_2 uptake across the range of temperatures that occur in the tundra biome. This indicates a shift from the historic state of tundra as a CO_2 sink.

Early analysis of Alaskan tundra reported a shift in growing season CO_2 balance from a historic C sink to a C source in response to warming and drying (Oechel *et al.* 1993). As more flux data were compiled from Alaskan tundra, across-site CO_2 balance was measured as net CO_2 uptake during the growing season. It was hypothesized that tundra ecosystems could have initially lost CO_2 in response to warming, then metabolically adjusted to continued warming while subsequently increasing CO_2 sink activity (Oechel *et al.* 2000). Our analysis using linear models does not allow us to quantify short-term fluctuations in source and sink activity, and data limitations preclude us from quantifying growing season trends in the early part of the record.

While we do not refute early data from Alaskan sites, we do not believe our pre-1990 growing season trend of CO_2 emissions adds any information useful for assessing this period. However, our larger post-1990 dataset clearly shows an increasing trend of growing season CO_2 uptake (Figure 4-2A). Our meta-analysis over a longer time period and from 32 sites across the tundra biome shows a more gradual and continuing increase in CO_2 uptake during the growing season, on average, through the modern period.

Similar to our finding of increased net growing season CO_2 uptake, recent studies have reported that tundra was a growing season CO_2 sink during the past two decades (McGuire *et al.* 2012; Ueyama *et al.* in press), with increasing CO_2 uptake in a majority of tundra sites in the 2000s (McGuire *et al.* 2012). In addition, long-term (since the early 1980s) remote sensing observations show a greening Arctic (Myneni *et al.* 1997; Jia & Epstein 2003; Nemani *et al.* 2003; Goetz *et al.* 2005; Sitch *et al.* 2007; Jia *et al.* 2009) and increased shrub encroachment (Stow *et al.* 2004; Sturm *et al.* 2005), both suggesting a regional response of accelerated C uptake by tundra vegetation. By extrapolating our post-1990 growing season trend to the areal extent of tundra (10.5×10^6 km^2; (McGuire *et al.* 1997; Callaghan *et al.* 2004), we estimate that tundra on average sequestered 137±80 Tg C during the growing seasons of the last few decades (1990-2006).

Winter CO_2 trends were less clear in our analysis across the entire data set, but the last 7 years of the record show a strong increase in CO_2 emissions (Figure 4-2B). We acknowledge that the estimated slope from a 7-year trend may not match a decadal-scale trend; based on the entire record it appears that the 7-year slope is likely an overestimate of longer trends (Figure 4-2B). This variability highlights the great need for additional sustained winter data to strengthen this record. Summing the growing season and longer-term winter trend, we estimated that tundra

sites were CO_2 sources during the 1990s, but we were unable to differentiate tundra from carbon neutral during the 2000s (Figure 4-3). Using only the more recent 7-year winter trend predicts increasing CO_2 emission annually for the most recent time period (Figure 4-3B), and the increasing winter and annual temperature trends (Figure 4-5) indicate that recent increases of arctic air temperature should lead to an increase in annual CO_2 emissions.

Diverse lines of evidence support an amplification of the tundra C cycle in recent decades, but large uncertainty in past estimates have impeded the ability to accurately determine the annual C balance. Top-down atmospheric inversion studies show the Arctic as a C sink (-410±400 Tg C y^{-1}) during the 1990s (Baker *et al.* 2006; McGuire *et al.* 2009), although recent inversion analyses were unable to distinguish Arctic tundra from C neutral in the 1990s (-13; range=-321 to 140 Tg C yr^{-1}) or the 2000s (-117; range=-439 to 243 Tg C yr^{-1}; (McGuire *et al.* 2012). Retrospective analyses from process-based models show an amplification of tundra C uptake and C emissions, but in the last few decades predict that tundra is a C sink. However, model predictions vary in sink strength and exhibit large temporal and spatial variability in source and sink activity (Clein *et al.* 2000; McGuire *et al.* 2000; Sitch *et al.* 2003; Sitch *et al.* 2007; Grant *et al.* 2011). In a recent comparative analysis McGuire et al. (2012) found that summed estimates of annual C fluxes over the past few decades (1990-2006) from inversion models (-96; range=-331 to 173 Tg C yr^{-1}) were C neutral, while regional (-177; range=-284 to -41 Tg C yr^{-1}) and global (-86; range=-205 to -1 Tg C yr^{-1}) process-based models predicted that tundra was a C sink, although sink strength could not be determined due to uncertainty in estimates (McGuire *et al.* 2012). In addition, they reported that observationally based estimates of annual CO_2 balance over the last two decades ranged from C neutral (10; range=-10 to 28 Tg C yr^{-1}) to a weak C sink (-82; range=-134 to -30 Tg C yr^{-1}; (McGuire *et al.* 2012). In contrast,

our mean annual estimate (Figure 4-3A) extrapolated to the areal extent of tundra from the same time period predicts tundra was a CO_2 source (462±378 Tg C yr^{-1}). The divergence of these observationally based estimates could be due to the larger variation in vegetation types and sampling duration and frequency of studies included in the McGuire et al (2012) meta-analysis.

For tundra to be a historic C sink over centuries to millennia, C uptake had to be greater than C emissions across the range of conditions within the biome. Yet our annual temperature response based on the past several decades of measurements predicts that tundra sites are CO_2 sources across the range of temperatures (Figure 4-5). Within this range, tundra sites with warmer temperatures exhibit greater CO_2 fluxes (Figure 4-4; (Ueyama *et al.* in press)) and both CO_2 uptake and CO_2 emissions are amplified by temperature a similar rate. These results suggest there has been a shift from the historic equilibrium and now C uptake and C emissions are of different magnitudes, with C emissions dominating across the range of conditions on an annual basis. These predictions are supported by recent flux studies (2008-2010) from relatively warm (long-term MAT of -1C) and cold (long-term MAT of -12) tundra sites, which report CO_2 losses in five out of six annual observations ranging from 13-78 g C m^{-2} yr^{-1} and 2-82 g C m^{-2} yr^{-1}, respectively (Belshe *et al.* 2012; Euskirchen *et al.* 2012).

A combination of several factors may have shifted the C balance of tundra ecosystems in recent decades. Surface air temperature has increased 0.35ºC per decade since the 1970s, with dramatic increases since the 1990s (Polyakov *et al.* 2002; Hinzman *et al.* 2005; Serreze & Francis 2006; Euskirchen *et al.* 2007; McGuire *et al.* 2009), atmospheric CO_2 has increased by 50 ppm since 1980 (Keeling & Whorf 2005) NOAA/ESLR), and the rate and areal extent of permafrost thaw has dramatically increased (Jorgenson *et al.* 2001; Stow *et al.* 2004; Hinzman *et al.* 2005; Schuur *et al.* 2008; Osterkamp *et al.* 2009). This analysis indicates that tundra

ecosystems have not completely acclimated to recent changes and are currently undergoing a multi-decade transition. In this transient state these ecosystems are CO_2 sources because of the unequal magnitude of CO_2 uptake and emissions. Based on our predicted annual temperature response, CO_2 emissions should exceed CO_2 uptake and push tundra to a CO_2 source on an annual basis, if they are not already doing so. Although our annual temporal trend is not definitive throughout the entire 40-year period, these data taken together suggest that despite increases in growing season CO_2 uptake, tundra ecosystems are currently CO_2 sources on an annual basis.

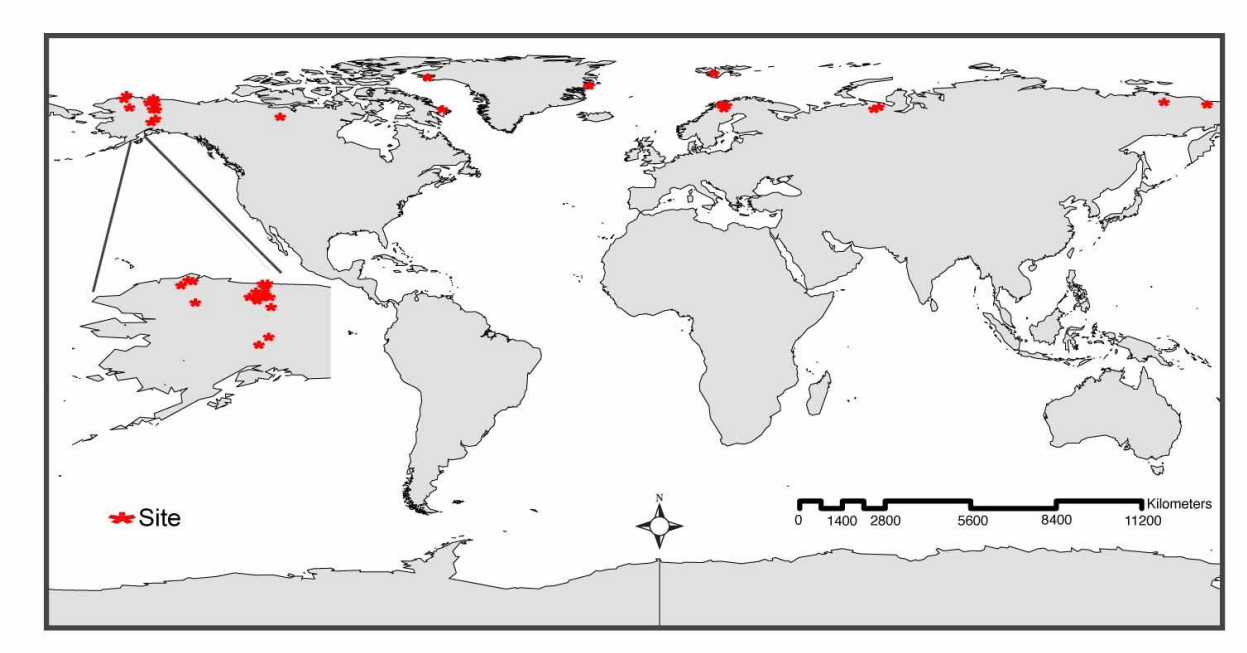

Figure 4-1. Map of the World showing the 32 sites (stars) included in this meta-analysis.

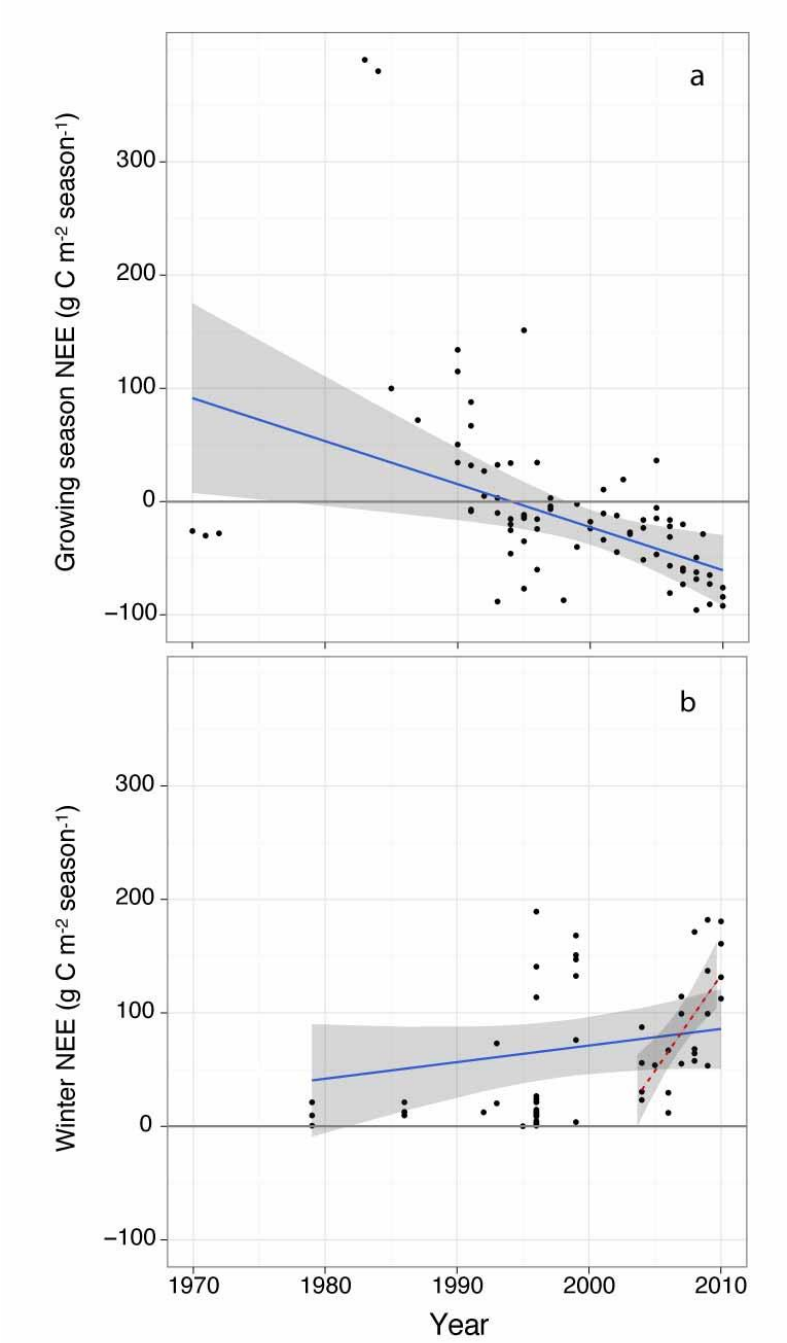

Figure 4-2. Temporal trends of net ecosystem CO_2 exchange (g C m^{-2} yr^{-1}). (A) During the growing season (-3.8±1.4 g C m^{-2} yr^{-1}; p =0.03). (B) During the winter with the long-term winter trend (1.5±1.1 g C m^{-2} yr^{-1}; p=0.18) shown in solid blue and the most recent 7-year winter trend (15.9±4.3 g C m-2 yr^{-1}; p=0.03) in dashed red. Estimates of slopes are reported with standard errors; positive values denote a C source. The trend lines shown are from simple linear models, but slope estimates are based on the full mixed-effect models.

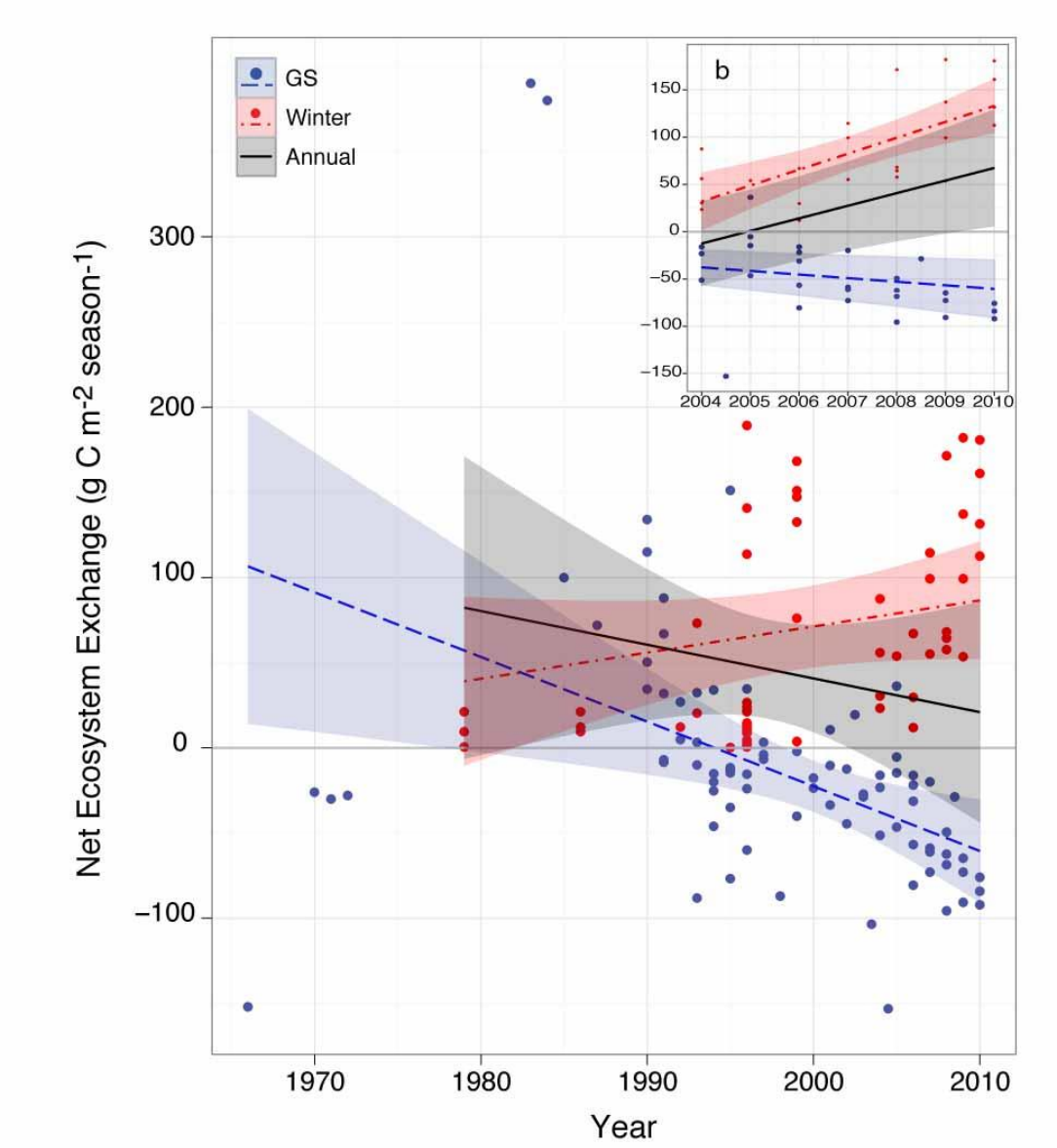

Figure 4-3. Estimates of temporal trends of net ecosystem exchange (g C m^{-2} $season^{-1}$) of CO_2. (A) For the entire data record during the growing season (GS; blue), winter (red), and the annual period (black; produced by summing predicted values of seasonal trends and their variances). (B) Temporal trends of GS, winter, and annual periods estimated from the last 7 years of the record. Trend lines are reported with 95% confidence intervals and are based on predictions from full mixed-effect models; positive values denote a C source.

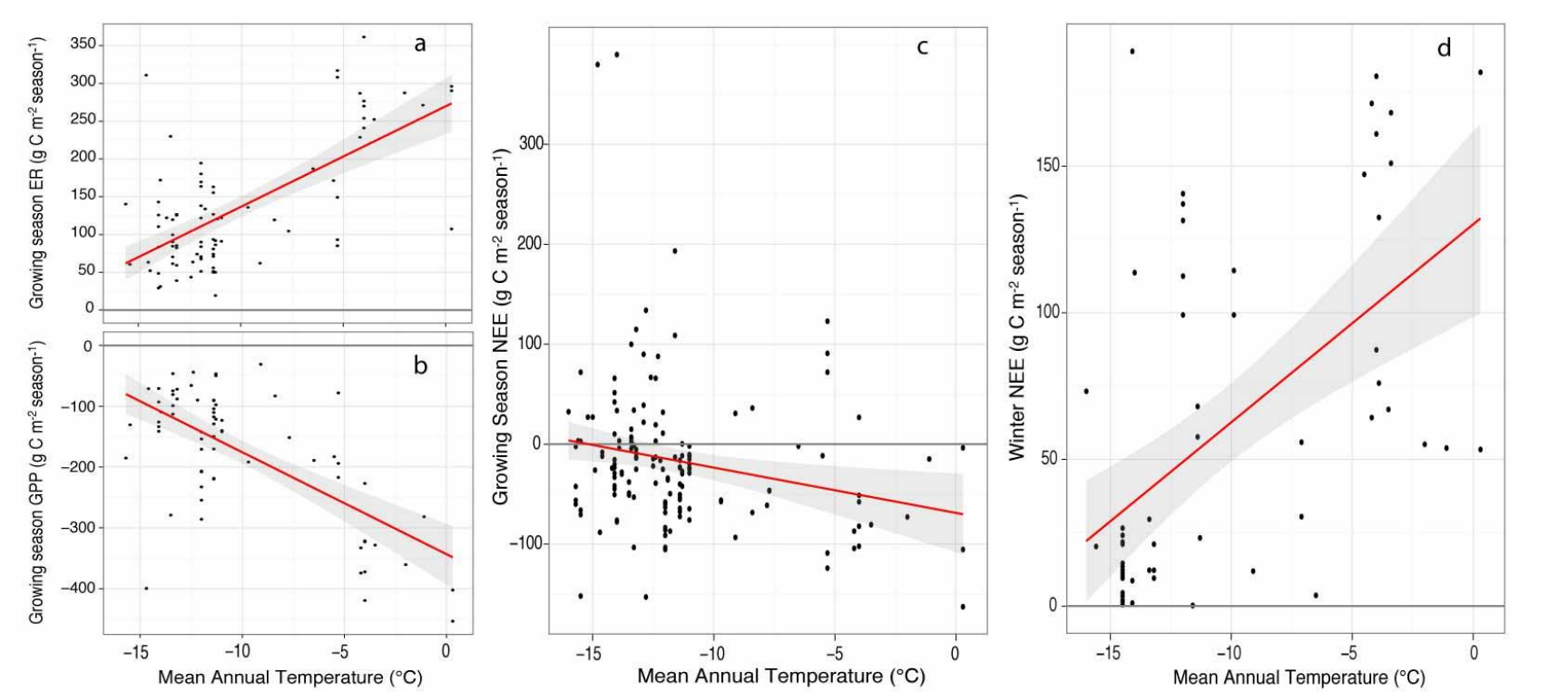

Figure 4-4. Linear relationships between mean annual temperature and carbon fluxes. (A) Growing season ecosystem respiration (ER; est.=13.3±1.6; p=0.001; adj. R^2=0.45). (B) Growing season gross primary production (GPP; est.=-16.7±2.3; p=0.001; adj. R^2=0.43). (C) Growing season net ecosystem exchange (NEE; est.=-4.5±1.7; p=0.007; adj. R^2=0.04). (D) Winter net ecosystem exchange (est.=6.8±1.3; p =0.001; adj. R^2=0.31). Estimates of slopes are reported with standard errors; positive values denote a C source.

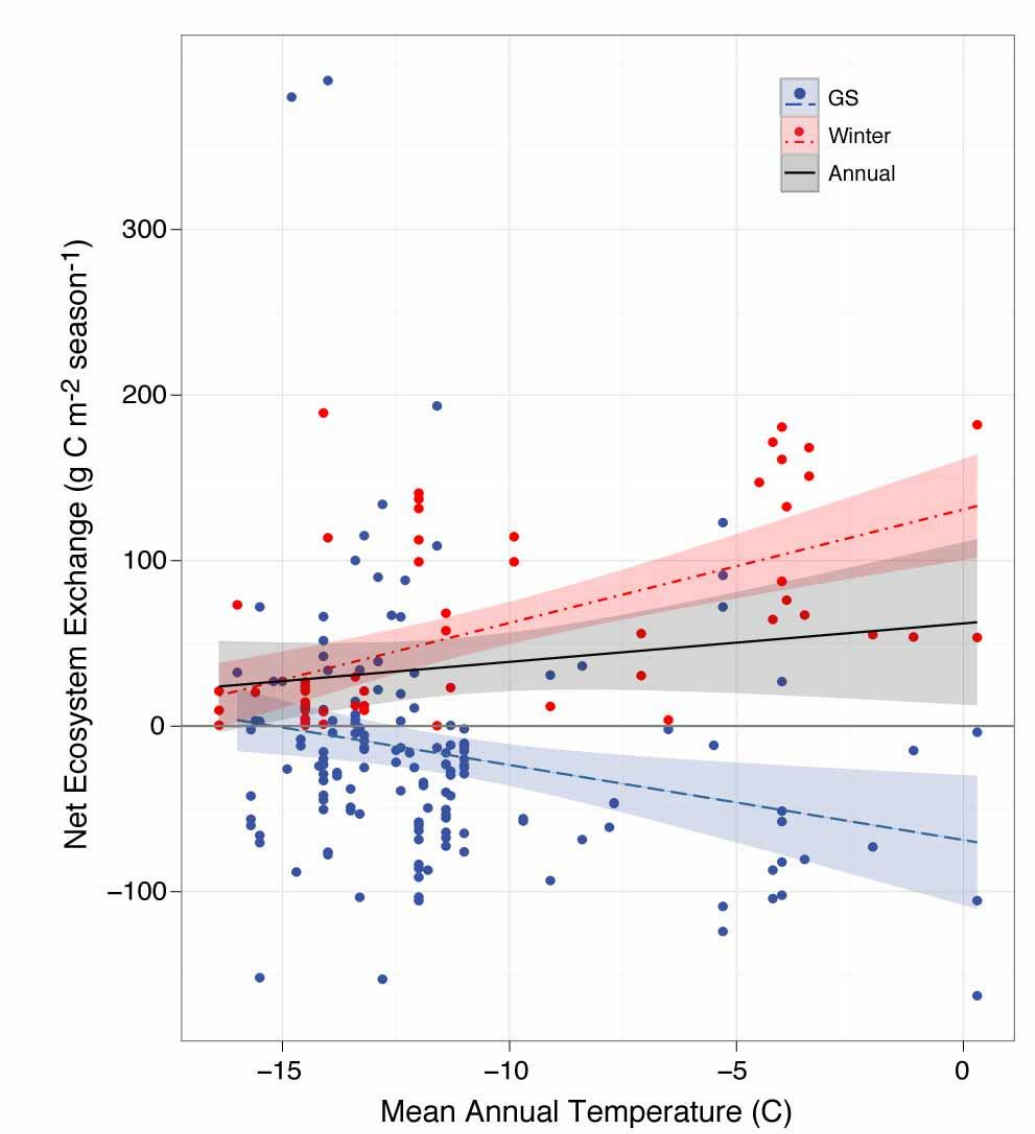

Figure 4-5. Estimates of linear relationships between mean annual temperature (°C) and net ecosystem exchange (g C m^{-2} $season^{-1}$) of CO_2 during the growing season (GS; blue), and winter (red) with 95% confidence intervals, and the annual estimate (black) of the temperature relationship produced by summing predicted values of seasonal trends and their variances. Positive values denote a C source.

CHAPTER 5
CONCLUSION

Temperature is increasing in high-latitude ecosystems and permafrost is dynamically shifting to be in equilibrium with contemporary climate (Chapin et al., 2005, Jorgenson et al., 2006, Camill, 2005, Hinzman et al., 2005, Osterkamp et al., 2009, Romanovsky et al., 2010, Schuur et al., 2008). In response to warming, soil active layers are thickening and thermokarst are forming, which creates a diversity of landforms that alter the physical environment in dynamic ways (Hinzman et al., 2005, Jorgenson and Osterkamp, 2005, Anisimov et al., 2007, Grosse et al., 2011). These physical changes feed back to affect biological and biochemical processes, which ultimately alter the cycling of carbon through high-latitude ecosystems. Because of the large accumulation of soil carbon in this region and the potential for its release to the atmosphere (Schuur et al., 2008, Tarnocai et al., 2009), it is imperative to develop ways to quantify both the spatial variation created by permafrost thaw and its effect on carbon fluxes.

For this dissertation, I focused on a particular type of thermokarst features (thermokarst gullies) that have formed within the Eight Mile Lake (EML) watershed and are typical and abundant in upland tundra landscapes. I detected and mapped these small, irregular thermokarst features by preforming a supervised classification on a high-resolution IKONOS image. I found that twelve percent of the EML watershed has undergone subsidence and thermokarst features predominantly form in valleys where tussock tundra resides. By 2008, 35% of the 3.7 km^2 tussock tundra class had transitioned to thermokarst. These landscape level changes created by permafrost thaw at EML have important implications for its carbon cycle because thermokarst features are forming in soil carbon rich areas and are altering the hydrology in ways that increase seasonal thawing of the soil.

To better quantify how permafrost thaw effects the carbon balance of tundra at EML, I developed a modeling technique to incorporate spatial differences in microtopography largely due to thermokarst subsidence into a carbon estimate. Net ecosystem exchange (NEE) of carbon was measured using eddy covariance (EC), during two 6-month campaigns in 2008 and 2009, and a spatially explicit quantitative metric of permafrost thaw based on variation in microtopography was developed. This spatial variation was incorporated into an EC carbon flux estimate using a generalized additive model (GAM), which allowed us to make predictions about carbon exchange for the landscape as a whole, and for specific landscape patches throughout the continuum of permafrost thaw and ground subsidence. In these study years, permafrost thaw appeared to increase the amplitude of the carbon cycle by stimulating both carbon release and sequestration, while the ecosystem remained a carbon sink at the landscape scale. Although we found the ecosystem was a carbon sink during the measurement campaigns of both years, this is not representative of the annual carbon balance because we did not measure carbon flux during a portion of the winter season. By linearly extrapolating between these missing winter periods, we found that annually the ecosystem became a carbon source of 60 $gCm^{-2}year^{-1}$ and 13 $gCm^{-2}year^{-1}$ in 2008 and 2009, respectively.

To put these results into a broader context and determine if regionally tundra carbon balance has changed in recent decades I compile 40 years of CO_2 flux observations from 54 studies spanning 32 sites across northern high latitudes. Using time-series analysis, I investigated if seasonal or annual CO_2 fluxes have changed over time, and whether spatial differences in mean annual temperature could help explain temporal changes in CO_2 flux. Growing season net CO_2 uptake has definitely increased since the 1990s; the data also suggest (albeit less definitively) an increase in winter CO_2 emissions, especially in the last decade. In spite of the

uncertainty in the winter trend, tundra sites were annual CO_2 sources from the mid-1980s until the 2000s; and data from the last seven years show that tundra continue to emit CO_2 annually. In addition, CO_2 emissions exceed CO_2 uptake across the range of temperatures that occur in the tundra biome. Taken together, these data suggest that despite increases in growing season uptake, tundra ecosystems are currently CO_2 sources on an annual basis.

Overall, the results from this work show that changes to permafrost are altering the landscape, and ultimately feeding back to amplify carbon cycling within upland tundra in central Alaska. Although this work does not directly link permafrost degradation to the regional shift of tundra from a historic sink to a CO_2 source, the site-level data points to this as a potential mechanism. Continued work is needed to fully understand and quantify the changes occurring to the carbon cycle as the landscape adjust to a warmer world. To better quantify annual carbon fluxes, more winter fluxes from a wider number of sites are needed. This will allow for better annual estimates and enable the detection of temporal changes in winter fluxes. In addition to improved quantification of carbon fluxes, higher resolution digital elevation models and other spatial products are needed to facilitate the detection of the spatial variation created by permafrost thaw using remotely sensed images.

Broadly, this dissertation work tries to understand how climate change, and the spatial variation created by permafrost thaw, feed back to alter the carbon cycle in high latitude ecosystems. This is a difficult question because there are tremendous amounts of spatial variation across the vast region underlain by permafrost in conjunction with spatial and temporal variation in changes in climate. My work has taken an empirical approach and by looking at patterns in observational data I have attempted to elucidate if with current data we can detect changes occurring in the carbon cycle of tundra ecosystems. This work is in contrast to more mechanistic

studies that are focused on the determination of specific mechanisms that result in detected changes. It takes a combination of these two types of work to start to answer the difficult question of how the carbon cycle will change in a warmer world.

LIST OF REFERENCES

Anderson D.R., Burnham K.P. & White G.C. (1998). Comparison of Akaike information criterion and consistent Akaike information criterion for model selection and statistical inference from capture-recapture studies. *J Appl Stat*, 25, 263-282.

Anderson D.R., Burnham K.P. & White G.C. (2001). Kullback-Leibler information in resolving natural resource conflicts when definitive data exist. *Wildlife Soc B*, 29, 1260-1270.

Anisimov O., Lobanov V., Reneva S., Shiklomanov N., Zhang T. & Nelson F. (2007). Uncertainties in gridded air temperature fields and effects on predictive active layer modeling. *Journal of Geophysical Research-Earth Surface*, 112, F02S14.

Anisimov O. & Nelson F. (1996). Permafrost distribution in the Northern Hemisphere under scenarios of climatic change. *Global and Planetary Change*, 14, 59-72.

Arens S., Sullivan P.F. & Welker J.M. (2008). Nonlinear responses to nitrogen and strong interactions with nitrogen and phosphorus additions drastically alter the structure and function of a high arctic …. *Journal of Geophysical Research*, 113, G03S09.

Aubinet M., Grelle A., Ibrom A., Rannik U., Moncrieff J., Foken T., Kowalski A.S., Martin P.H., Berbigier P., Bernhofer C., Clement R., Elbers J., Granier A., Grunwald T., Morgenstern K., Pilegaard K., Rebmann C., Snijders W., Valentini R. & Vesala T. (2000). Estimates of the annual net carbon and water exchange of forests: The EUROFLUX methodology. *Adv Ecol Res*, 30, 113-175.

Aubinet M., Heinesch B. & Longdoz B. (2002). Estimation of the carbon sequestration by a heterogeneous forest: night flux corrections, heterogeneity of the site and inter-annual variability. *Global Change Biology*, 8, 1053-1071.

Baker D.F., Peylin P., Law R.M., Gurney K.R., Rayner P., Denning A.S., Bousquet P., Bruhwiler L., Chen Y.H., Ciasis P., Fung I., Heimann M., John J., Maki T., Maksyutov S., Masarie K., Prater M., Pak B., Taguchi S. & Zhu Z. (2006). TransCom 3 inversion intercomparison: impact of transport model errors on the interannual variability of regional CO2 fluxes, 1988-2003. *Global Biogeochemical Cycles*, 20, 1002.

Baldocchi D. (2003). Assessing the eddy covariance technique for evaluating carbon dioxide exchange rates of ecosystems: past, present and future. *Global Change Biology*, 9, 479-492.

Belshe E.F., Schuur E.A.G., Bolker B.M. & Bracho R. (2012). Incorporating Spatial Heterogeneity Created by Permafrost Thaw into a Landscape Carbon Estimate. *Journal of Geophysical Research: Biogeosciences*, 117.

Beyer H.L. (2004). Hawth's Analysis Tools for ArcGIS.

Billings W. (1987). Carbon balance of Alaskan tundra and tiaga ecosystems: past, present, and future. *Quaternary Science Reviews*, 6, 165-177.

Boelman N., Stieglitz M., Rueth H., Sommerkorn M., Griffin K., Shaver G. & Gamon J. (2003). Response of NDVI, biomass, and ecosystem gas exchange to long-term warming and fertilization in wet sedge tundra. *Oecologia*, 135, 414-421.

Bolker B.M. (2010). bbmle: Tools for general maximum likelihood estimation.

Bonan G.B. (2002). *Ecological Climatology*. Cambridge University Press.

Booth J. (1995). Bootstrap methods for generalized linear mixed models with applications to small area estimation. In: *Statistical Modeling* (ed. Seeber GUH, B.J. Francis, R. Hatzinger, G. Steckel-Berger,). Springer New York, NY, pp. 43-51.

Brown J., Ferrians O.J., Heginbottom J.A. & Melnikov E.S. (1998). International Permafrost Association circum Arctic map of permafrost and ground-ice conditions. In. U.S. Geological Survey.

Burba G.G., Anderson D.J., L. X. & McDermitt D.K. (2008). Addressing the influence of instrument surface heat exchange on the measurments of CO2 flux form open-path gas analyzers. *Global Change Biology*, 14, 1854-1876.

Callaghan T., Bjorn L., Chernov Y., Chapin T., Christensen T., Huntley B., Ims R., Johansson M., Jolly D., Jonasson S., Matveyeva N., Panikov N., Oechel W. & Shaver G. (2004). Effects on the function of arctic ecosystems in the short- and long-term perspectives. *Ambio*, 33, 448-458.

Camill P. (2005). Permafrost thaw accelerates in Boreal peatlands during late-20th century climate warming. *Climate Change*, 68, 135-152.

Chapin F., Miller P.C., Billings W.D. & Coyne P.I. (1980). Carbon and nutrient budgets and their control in coastal tundra. In: *An arctic tundra ecosystem. The coastal tundra at Barrow, Alaska.* (eds. Brown J, Miller P, LL T & Bunnell F). Dowden Hutchinson and Ross Stroudsburg, Pennsylvania, pp. 458-482.

Chapin F., Sturm M., Serreze M.C., McFadden J.P., Key J.R., Lloyd A.H., McGuire A.D., Rupp T.S., Lynch A.H., Schimel J.P., Beringer J., Chapman W.L., Epstein H.E., Euskirchen E.S., Hinzman L.D., Jai G., Ping C.L., Tape K.D., Thompson C.D.C., Walker D.A. & Welker J.M. (2005). Role of Land-Surface Changes in Arctic Summer. *science*, 310, 657-660.

Chapin F.S., Eugster W., McFadden J.P., Lynch A.H. & Walker D.A. (2000). Summer differences among arctic ecosystems in regional climate forcing. *Journal of Climate*, 13, 12.

Chapin F.S. & Shaver G. (1996). Physiological and growth responses of Arctic plants to a field experiment simulating climate change. *Ecology*, 77, 822-840.

Clark K.L., Gholz H.L., Moncrieff J.B., Cropley F. & Loescher H.W. (1999). Environmental controls over net exchanges of carbon dioxide from contrasting Florida ecosystems. *Ecological Applications*, 9, 936-948.

Clein J.S., B. Kwiatkowski, A.D. McGuire, J.E. Hobbie, E.B. Rastetter, J.M. Melillo & Kicklighter D.W. (2000). Modeling carbon responses of tundra ecosystems to historical and projected climate: a comparison of a plot- and a global-scale ecosystem model to identify process-based uncertainties. *Global Change Biology*, 6, 127-140.

Congalton R.G. & Green K. (1999). *Assessing the accuracy of remotely sensed data: Principles and practices*. Lewis Publishers, Boca Raton, Florida.

Coyne P.I., J.J. Kelley (1975). CO2 exchange over the Alaskan arctic tundra: meteorological assessment by an aerodynamic method. *Journal of Applied Ecology*, 12, 587-661.

Davidson E., Belk E. & Boone R. (2002). Soil water content and temperature as independent or confounded factors controlling soil respiration in a temperate mixed hardwood forest. *Global Change Biology*, 4, 217-227.

Davidson E. & Janssens I. (2006). Temperature sensitivity of soil carbon decomposition and feedbacks to climate change. *Nature*, 440, 165-173.

Davis N. (2001). *Permafrost: A guide to frozen ground in transition.* University of Alaska Press, Fairbanks, AK.

Dioumaeva I., Trumbore S., Schuur E., Goulden M., Litvak M. & Hirsch A. (2003). Decomposition of peat from upland boreal forest: Temperature dependence and sources of respited carbon: Comparison of carbon exchange between boreal black spruce forest and the atmosphere for a wildfire age sequence. *Journal of Geophysical Research*, 108, WFX3.1-WFX3.12.

Dormann C.F. (2007). Effects of incorporating spatial autocorrelation into the analysis of species distribution data. *Global Ecology and Biogeography*, 16, 129-138.

Epstein H.E., Beringer J., Gould W., Lloyd A.H., Thompson C.D., Chapin F.S., Michaelson G.L., Ping C.L., Rupp T.S. & Walker D.A. (2004). The nature of spatial transitions in the Arctic. *Journal of Biogeography*, 31, 1917-1933.

Euskirchen E.S., Bret-Harte M.S., Scott G.L., Edgar C. & Shaver G.R. (2012). Seasonal patterns of carbon dioxide and water fluxes in three representative tundra ecosystems in northern Alaska. *Ecosphere*, 3.

Euskirchen S.E., McGuire A.D. & Chapin III F.S. (2007). Energy feedbacks of northern high-latitude ecosystems to the climate system due to reduced snow cover during the 20th century warming. *Global Change Biology*, 13, 2425-2438.

Fahnestock J., Jones M., Brooks P., Walker D.A. & Welker J.M. (1998). Winter and early spring CO2 efflux from tundra communities of northern Alaska. *Journal of Geophysical Research*, 103, 29023-29027.

Fahnestock J., Jones M. & Welker J.M. (1999). Wintertime CO2 efflux from Arctic soils: implications for annual carbon budgets. *Global Biogeochemical Cycles*, 13, 775-779.

Falge E., Baldocchi D., Olson R., Anthoni P., Aubinet M., Bernhofer C., Burba G., Ceulemans R., Clement R. & Dolman H. (2001). Gap filling strategies for defensible annual sums of net ecosystem exchange* 1. *Agricultural and forest meteorology*, 107, 43-69.

Giblin A., K. Nadelhoffer & G. Shaver (1991). Biogeochemical diversity along a riverside toposequence in arctic Alaska. *Ecological Monographs*, 61, 415-435.

Godin E. & Fortier D. (2012). Geomorphology of a thermo-erosion gully, Bylot Island, Nunavut, Canada. *Canadian Journal of Earth Science*, 49, 979-986.

Goetz S., Bunn A.G., Fiske G.L. & Houghton R.A. (2005). Satellite-observed photosynthetic trends across boreal North America associated with climate and fire disturbance. *Proceedings of the National Academy of Sciences of the United States of America*, 102, 13521.

Goulden M., Munger J., Fan S., Daube B. & Wofsy S. (1996). Measurements of carbon sequestration by long-term eddy covariance: methods and a critical evaluation of accuracy. *Global Change Biology*, 2, 169-182.

Goulden M.L., Wofsy S.C., Harden J., Trumbore S., Crill P.M., Gower S.T., Fries T., Daube B.C., S.-M. F., Sutton D.J., Bazzaz A. & Munger J.W. (1998). Sensitivity of boreal forest carbon balance to soil thaw. *Science*, 279, 214-217.

Goward S., Tucker C. & Dye D. (1985). North American vegetation patterns observed with the NOAA-7 advanced very high resolution radiometer. *Vegetation*, 64, 3-14.

Grant R.F., Humphreys E.R., Lafleur P.M. & Dimitrov D.D. (2011). Ecological controls on net ecosystem productivity of a mesic arctic tundra under current and future climates. *Journal Of Geophysical Research-Biogeosciences*, 116, G01031.

Groendahl L., Friborg T. & Soegaard H. (2007). Temperature and snow-melt controls on interannual variability in carbon exchange in the high Arctic. *Theoretical and Applied Climatology*, 88.

Grogan P. & Chapin F.S. (1999). Arctic soil respiration: effects of climate and vegetation depend on season. *Ecosystems*, 2, 451-459.

Grogan P. & Jonasson S. (2006). Ecosystem CO2 production during winter in a Swedish subarctic region: the relative importance of climate and vegetation type. *Global Change Biology*, 12, 1479-1495.

Grosse G., Harden J., Turetsky M., McGuire A.D., Camill P., Tarnocai C., Frolking S., Schuur E.A.G., Jorgenson T., Marchenko S., Romanovsky V., Wickland K.P., French N., Waldrop M., Bourgeau-Chavez L. & Striegl R.G. (2011). Vulnerability of high-latitude soil organic carbon in North America to distribance. *Journal of Geophysical Research,* 116.

Grulke N., G. Riechers, W. Oechel & U. Hjelm (1990). Carbon balance in tussock tundra under ambient and elevated atmospheric CO 2. *Oecologia*, 83.

Harazono Y., M. Mano, A. Miyata & R. Zulueta (2003). Inter- annual carbon dioxide uptake of a wet sedge tundra ecosystem in the Arctic. *Tellus Series B-Chemical And Physical Meteorology*, 55B, 215-231.

Harden J., Mark R.K., Sundquist E.T. & Stallard R.F. (1992). Dynamics of soil carbon during deglaciation of the Laurentide ice sheet. *Science*, 258, 1921-1924.

Hastie T.J. & Tibshirani R.J. (1990). *Generalized Additive Models*. Chapman and Hall/CRC, Boca Raton.

Heikkinen J., V. Elsakov & Martikainem P.J. (2002). Carbon dioxide and methane dynamics and annual carbon balance in tundra wetland in NE Europe, Russia. *Global Biogeochemical Cycles*, 16, 1115.

Heikkinen J.E.P., T. Virtanen, J.T. Huttunen, V. Elsakov & Martikainen P.J. (2004). Carbon balance in East European tundra. *Global Biogeochemical Cycles*, 18, GB1023.

Hicks Pries C.E., Schuur E.A.G. & Crummer K.G. (2012). Holocene carbon stocks and carbon accumulation rates altered in soils undergoing permafrost thaw. *Ecosystems*, 15, 162-173.

Hinkel K.M., Eisner W.R., Bockheim J.G., Nelson F.E., Peterson K.M. & Dai X. (2003). Spatial extent, age, and carbon stocks in drained thaw lake basins on the Barrow Peninsula, Alaska. *Arctic, Antarctic, and Alpine Research*, 35, 291-300.

Hinkel K.M. & Hurd J.K. (2006). Permafrost destabilization and thermokarst following snow fence installation, Barrow, Alaska, USA. *Arct Antarct Alp Res*, 38, 530-539.

Hinzman L., Bettez N.D., Bolton W.R., Chapin F.S., Dyurgerov M.B., Fastie C.L., Griffith B., Hollister R.D., Hope A. & Huntington H.P. (2005). Evidence and implications of recent climate change in northern Alaska and other arctic regions. *Climatic Change*, 72, 251-298.

Hobbie S.E., F.S. Chapin III, (1998). The response of tundra plant biomass, aboveground production, nitrogen, and CO2 flux to experimental warming. *Ecology*, 79, 1526-1544.

Hobbie S.E., Schimel J.P., Trumbore S.E. & Randerson J.R. (2000). Controls over carbon storage and turnover in high-latitude soils. *Global Change Biology*, 6, 196-210.

Hollinger D.Y., Kelliher F.M., Byers J.N., Hunt J.E., Mcseveny T.M. & Weir P.L. (1994). Carbon-Dioxide Exchange between an Undisturbed Old-Growth Temperate Forest and the Atmosphere. *Ecology*, 75, 134-150.

Huemmrich K.F., Kinoshita G., Gamon J.A., Houston S., Kwon H. & Oechel W.C. (2010). Tundra carbon balance under varying temperature and moisture regimes. *Journal Of Geophysical Research-Biogeosciences*, 115, G00I02.

Humphreys E.R. & Lafleur P.M. (2011). Does earlier snowmelt lead to greater CO 2sequestration in two low Arctic tundra ecosystems? *Geophysical Research Letters*, 38, L09703.

IPCC (2007). *Climate Change 2007: The Physical Science Basis. Contribution of Working Group 1 to the Fouth Assesment Report of the Intergovernmental Panel on Climate Change*. Cambridge University Press, Cambridge, UK / New York, NY.

Jafarov E.E., Marchenko S.S. & Romanovsky V.E. (2012). Numerical modeling of permafrost dynamics in Alaska using a high spatial resolution dataset. *The Cryosphere Discussions*, 6, 89-124.

Jensen J.R. (2005). *Introductory digital image processing: A remote sensing perspective*. 3rd edn. Pearson Education, Inc., Upper Saddle River, NJ.

Jia G. & Epstein H. (2003). Greening of arctic Alaska. 1981-2001. *Geophysical Research Letters*, 30, 2067.

Jia G., Epstein H. & Walker D.A. (2009). Vegetation greening in the canadian arctic related to decadal warming. *Journal of Environmental Monitoring*, 11, 2231-2238.

Johnson L., Shaver G., Cades D., Rastetter E., Nadelhoffer K., Giblin A., Laundre J. & Stanley A. (2000). Plant carbon-nutrient interactions control CO2 exchange in Alaskan wet sedge tundra ecosystems. *Ecology*.

Johnson P.L., J.J. Kelley (1970). Dynamics of carbon dioxide and productivity in an arctic biosphere. *Ecology*, 51, 73-80.

Jones B.M., Grosse G., Arp C.D., Jones M.C., Walter Anthony K. & Romanovsky V. (2011). Modern thermokarst lake dynamics in the continuous permafrost zone, northern Seward Peninsula, Alaska. *Journal of Geophysical Research*, 116, G00M03.

Jones M., Fahnestock J. & Welker J.M. (1999). Early and late winter CO 2 efflux from arctic tundra in the Kuparuk River watershed, Alaska, USA. *Arctic, Antarctic, and Alpine Research*, 31, 187-190.

Jones M.C., Grosse G., Jones B.M. & Walter Anthony K. (2012). Peat accumulation in drained thermokarst lake basins in continuous, ice-rich permafrost, northern Seward Peninsula, Alaska. *Journal of Geophysical Research*, 117.

Jorgenson M. & Osterkamp T. (2005). Response of boreal ecosystems to varying modes of permafrost degradation. *Canadian Journal of Forest Research*, 35, 2100-2111.

Jorgenson M.T., Racine C.H., Walters J.C. & Osterkamp T.E. (2001). Permafrost Degradation and Ecological Changes Associated with a WarmingClimate in Central Alaska. *Climatic Change*, 48, 551-579.

Jorgenson M.T., Shur Y.L. & Pullman E.R. (2006). Abrupt increase in permafrost degradation in Arctic Alaska. *Geophysical Research Letters*, 33.

Kane D., Hinkel K., Goering D., Hinzman L. & Outcalt S. (2001). Non-conductive heat transfer associated with frozen soils. *Global and Planetary Change*, 29, 275-292.

Keeling C.D. & Whorf T.P. (2005). Atmospheric CO2 records from sites in the SIO air sampling network. In: *In trends: A compendium of data on global change.* Carbon dioxide information Analysis Center, Oak Ridge National Laboratory, U.S. Departmenf of Energy Oak Ridge, Tenn., U.S.A.

Kim Y.J. & Gu C. (2004). Smoothing spline Gaussian regression: more scalable computation via efficient approximation. *J Roy Stat Soc B*, 66, 337-356.

Kljun N., Kormann R., Rotach N. & Meixner F. (2003). Comparison of the langrangian footprint model LPDM-B with an analytical footprint model. *Bound-Lay Meteorol*, 106, 348-355.

Kormann R. & Meixner F. (2001). An analytical footprint model for non-neutral stratification. *Boundary-Layer Meteorol*, 99, 207-224.

Kutzbach L., Wille C. & Pfeiffer E.M. (2007). The exchange of carbon dioxide between wet arctic tundra and the atmosphere at the Lena River Delta, Northern Siberia. *Biogeosciences*, 4, 869-890.

Kwon H.-J., Oechel W.C., Zulueta R.C. & Hastings S.J. (2006). Effects of climate variability on carbon sequestration among adjacent wet sedge tundra and moist tussock tundra ecosystems. *Journal Of Geophysical Research-Biogeosciences*, 111, G03014.

La Puma I., Philippi T. & Oberbauer S. (2007). Relating NDVI to ecosystem CO2 exchange patterns in response to season length and soil warming manipulations in arctic Alaska. *Remote Sensing of Environment*, 109, 225-236.

Lafleur P.M. & Humphreys E.R. (2007). Spring warming and carbon dioxide exchange over low Arctic tundra in central Canada. *Global Change Biology*, 14, 740-756.

Laine A., Sottocornola M., Kiely G., Byrne K., Wilson D. & Tuittila E. (2006). Estimating net ecosystem exchange in a patterned ecosystem: example from blanket bog. *Agricultural and Forest Meteorology*, 138, 231-243.

Lantuit H., Pollard W.H., Couture N., Fritz M., Schirrmeister L., Meyer H. & Hubberten H -.W. (2012). Modern and Late Holocene retrogressive thaw slump activity on the Yukon

Coastal Plain and Herschel Island, Yukon Territory, Canada. *Permafrost and Periglacial Processes*, 23, 39-51.

Lantuit H. & Pollard W.H. (2008). Fifty years of coastal erosion and retrogressive thaw slump activity on Herschel Island, southern Beaufort Sea, Yukon Territory, Canada. *Geomorphology*, 95, 84-102.

Lawrence D.M., Slater A.G., Romanovsky V.E. & Nicolsky D.J. (2008). Sensitivity of a model projection of near-surface permafrost degradation to soil column depth and representation of soil organic matter. *Journal of Geophysical Research*, 113.

Lee H., Schuur E., Vogel J., Lavoie M., Bhadra D. & Staudhammer C. (2010). A spatially explicit analysis to extrapolate carbon fluxes in upland tundra where permafrost is thawing. *Global Change Biology*, 17, 1379-1393.

Liebethal C. & Foken T. (2007). Evaluation of six parameterization approaches for the estimation of ground heat flux. *Theoretical and Applied Climatology*, 88, 43-56.

Liebethal C., Huwe B. & Foken T. (2005). Sensitivity analysis for two ground heat flux calculation approaches. *Agricultural and Forest Meteorology*, 132, 253-262.

Lyons L. (1991). *A practical guide to data analysis for physical science students*. Cambridge University Press, Cambridge, England.

Mack M., Schuur E., Bret-Harte M., Shaver G. & Chapin III F. (2004). Ecosystem carbon storage in arctic tundra reduced by long-term nutrient fertilization. *Nature*.

McGuire A., Melillo J.M., Kicklighter D.W., Pan Y., Xiao X., Helfrich J., Morre III M.B., Vorosmarty C.J. & Schloss A.L. (1997). Equilibrium responses of global net primary productivity and carbon storage to doubled atmospheric carbon dioxide: Sensitivity to changes in vegetation nitrogen concentration. *Global Biogeochemical Cycles*, 11, 173-189.

McGuire A.D., Anderson L.G., Christensen T.R., Dallimore S., Guo L., Haynes D.J., Heimann M., Lorenson T.D., MacDonald R.W. & Roulet N. (2009). Sensitivity of the carbon cycle in the Arctic to climate change. *Ecological Monographs*, 79, 523-555.

McGuire A.D., Christensen T.R., Hayes D., Heroult A., Euskirchen E., Yi Y., Kimball J.S., Koven C., Lafleur P., Miller P.A., Oechel W., Peylin P. & Williams M. (2012). An assessment of the carbon balance of arctic tundra: comparisons among observations, proscess models, and atmospheric inversions. *Biogeosciences*, 9.

McGuire A.D., Clein J.S., Melillo J.M., Kicklighter D.W., Meier R.A., Vorosmarty C.J. & Serreze M.C. (2000). Modelling carbon responses of tundra ecosystems to historical and projected climate: sensitivity of pan-Arctic carbon storage to temporal and spatial variation in climate. *Global Change Biology*, 6, 141-159.

Michaelson G.L., Ping C.L. & Kimble J.M. (1996). Carbon storage and distribution in tundra soils of Arctic Alaska, USA. *Arctic Alpine Research*, 28.

Mikan C., Schimel J. & Doyle A. (2002). Temperature controls of microbial respiration in arctic tundra soils above and below freezing. *Soil Biology and Biochemistry*, 34, 1785-1795.

Miller P., Kendall R. & Oechel W.C. (1983). Simulating carbon accumulation in northern ecosystems. *Simulation*, 40, 119-131.

Moncrieff J.B., Massheder J.M., deBruin H., Elbers J., Friborg T., Heusinkveld B., Kabat P., Scott S., Soegaard H. & Verhoef A. (1997). A system to measure surface fluxes of momentum, sensible heat, water vapour and carbon dioxide. *J Hydrol*, 189, 589-611.

Morgenstern A., Grosse G., Gunther F., Fedorova I. & Schirrmeister L. (2011). Spatial analyses of thermokarst lakes and basins in Yedoma landscapes of the Lena Delta. *The Cryosphere* 5, 849-867.

Myneni R.B., Keeling C.D., Tucker C.J., Asrar G. & Nemani R.R. (1997). Increased plant growth in the northern high latitudes from 1981-1991. *Nature*, 386.

Natali S., Schuur E. & Rubin R. (in review). Increased plant productivity in Alaskan tundra with experimental warming of soil and permafrost. *Ecology*.

Nemani R.R., Keeling C.D., Hashimoto H., Molly W.M., Piper S.C., Tucker C.J., Myneni R.B. & Running S.W. (2003). Climate-driven increases in global terrestrial net primary production from 1982-1999. *Science*, 300.

Nobrega S. & Grogan P. (2007). Deeper snow enhances winter respiration from both plant-associated and bulk soil carbon pools in birch hummock tundra. *Ecosystems*, 10, 419-431.

Nobrega S. & Grogan P. (2008). Landscape and ecosystem-level controls on net carbon dioxide exchange along a natural moisture gradient in Canadian low arctic tundra. *Ecosystems*, 11, 377-396.

Oberbauer S., C. Gillespie, W. Cheng, A. Sala, R. Gebauer & J.D. Tenhunen (1996). Diurnal and seasonal patterns of ecosystem CO2 efflux from upland tundra in the foothills of the Brooks Range, Alaska, USA. *Arctic and Alpine Research*, 28, 328-338.

Oberbauer S., G. Starr & E.W. Pop (1998). Effects of extended growing season and soil warming on carbon dioxide and methane exchange of tussock tundra in Alaska. *Journal of Geophysical Research*, 103, 29075-29082.

Oberbauer S., Tenhunen J. & Reynolds J. (1991). Environmental effects on CO2 efflux from water track and tussock tundra in arctic Alaska, U.S.A. *Arctic and Alpine Research*, 23, 162-169.

Oechel W. & Billings W.D. (1992). Effects of global change on the carbon balance of arctic plants and ecosystems. In: *Arctic ecosystems in a changing climate: an ecophysiological*

perspective. (eds. Chapin III F, Jefferies R, Reynolds J, Shaver G & Svoboda J). Academic Press San Diego, CA, pp. 139-168.

Oechel W., G. Vourlitis & S.J. Hastings (1997). Cold season CO2 emission from arctic soils. *Global Biogeochemical Cycles*, 11, 163-172.

Oechel W., Hastings S.J., Vourlitis G., Jenkins M., Riechers G. & Grulke N. (1993). Recent change of Arctic tundra ecosystems from a net carbon dioxide sink to a source. *Nature*, 361, 520-523.

Oechel W., Vourlitis G. & Hastings S. (1995). Change in Arctic CO^ 2 Flux Over Two Decades: Effects of Climate Change at Barrow, Alaska. *Ecological Applications*, 5, 846-855.

Oechel W., Vourlitis G., Hastings S., Ault R.P. & Bryant P. (1998). The effects of water table manipulation and elevated temperature on the net CO2 flux of wet sedge tundra ecosystems. *Global Change Biology*, 4, 77-90.

Oechel W.C., Vourlitis G.L., Hastings S.J., Zulueta R.C., Hinzman L. & Kane D. (2000). Acclimation of ecosystem CO2 exchange in the Alaskan Arctic in response to decadal climate warming. *Nature*, 406, 978-981.

Olivas P., Oberbauer S., Tweedie C., Oechel W.C., Lin D. & Kuchy A. (2011). Effects of Fine-Scale Topography on CO 2 Flux Components of Alaskan Coastal Plain Tundra: Response to Contrasting Growing Seasons. *Arctic, Antarctic, and Alpine Research*, 43, 256-266.

Osterkamp T. (2005). The recent warming of permafrost in Alaska. *Global and Planetary Change*, 49, 187-202.

Osterkamp T.E., Jorgenson M.T., Schuur E.A.G., Shur Y.L., Kanevskiy M.Z., Vogel J.G. & Tumskoy V.E. (2009). Physical and Ecological Changes Associated with Warming Permafrost and Thermokarst in Interior Alaska. *Permafrost and Periglacial Processes*, 20, 235-256.

Pinheiro J., Bates D., Sarkar D. & R development Core Team (2011). *nlme: Linear and Nonlinear Mixed Effects Models*. R package version 3.1-98 edn.

Polyakov I.D., Alekseev G.V., Bekryacy R.V., Bhatt U., Colony R., Johnson M.A., Karklin V.P., Makshtas A.P., Walsh D. & Yulin Y.V. (2002). Observationally based assessment of polar amplification of global warming. *Geophysical Research Letters*, 29, 1878.

Poole D., P.C. Miller, (1982). Carbon dioxide flux from three Arctic tundra types in north-central Alaska, USA. *Arctic and Alpine Research*, 14, 27-32.

Post W. (1990). Report of a workshop on climate feedbacks and the role of peatlands, tundra, and boreal ecosystems in the global carbon cycle. In. Oak Ridge National Lab Oak Ridge, TN.

R Development Core Team (2010). R: A language and enviroment for statistical computing. URL http://www.R-project.org/

Raynolds M.K., Walker D.A. & Maier H.A. (2006). NDVI patterns and phytomass distribution in the circumpolar Arctic. *Remote Sensing of Environment*, 102, 271-281.

Reynolds O. (1985). On the dynamical theory of incompressible viscous fluids and the determination of the criterion. *Philosophical Transactions of the Royal Society A*, 186, 123-164.

Richardson A., Mahecha M., Falge E., Kattge J., Moffat A., Papale D., Reichstein M., Stauch V., Braswell B. & Churkina G. (2008). Statistical properties of random CO2 flux measurement uncertainty inferred from model residuals. *agricultural and forest meteorology*, 148, 38-50.

Rivkina E., Friedmann E., McKay C. & Gilichinsky D. (2000). Metabolic activity of permafrost bacteria below the freezing point. *Applied and Environmental Microbiology*, 3239-3233.

Rocha A. & Shaver G.R. (2011). Burn severity influences postfire CO2 exchange in arctic tundra. *Ecological Applications*, 21, 477-489.

Rogers M.C., Sullivan P.F. & Welker J.M. (2011). Evidence of Nonlinearity in the Response of Net Ecosystem CO 2 Exchange to Increasing Levels of Winter Snow Depth in the High Arctic of Northwest Greenland. *Arctic, Antarctic, and Alpine Research*, 43, 95-106.

Romanovsky V., Gruber S., Instanes A., Jin H., Marchenko S., Smith S., Trombotto D. & Walter K. (2007). Frozen Ground. In: *Global outlook for ice and snow* (ed. UNEP/GRID) Arendal, Norway.

Romanovsky V.E., Smith S.L. & Christiansen H.H. (2010). Permafrost thermal state in the polar Northern Hemisphere during the international polar year 2007-2009: a synthesis. *Permafrost and Periglacial Processes*, 21, 106-116.

Saito K., Kimoto M, Zhang T, Takata K & Emori S (2007). Evaluating a high-resolution climate model: Simulated hydrothermal regimes in frozen ground regions and their change under the global warming scenario. *J. Geophys. Res*, 112.

Schmid H. (1997). Experimental design for flux measurements: matching scales of observations and fluxes. *Agricultural and Forest Meteorology*, 87, 179-200.

Schmid H. (2002). Footprint modeling for vegetation atmosphere exchange studies: a review and perspective. *Agricultural and Forest Meteorology*, 113, 159-183.

Schmid H. & Lloyd C. (1998). Spatial representativeness and the location bias of flux footprints over inhomogeneous areas. *Agricultural and Forest Meteorology*, 93, 195.

Schuur E., Bockheim J., Canadell J.G., Euskirchen E., Field C.B., Goryachkin S.V., Hagemann S., Kuhry P., Lafleur P.M. & Lee H. (2008). Vulnerability of permafrost carbon to climate change: Implications for the global carbon cycle. *BioScience*, 58, 701-714.

Schuur E., J Vogel, K Crummer, H Lee, JO Sickman & TE Osterkamp (2009). The effect of permafrost thaw on old carbon release and net carbon exchange from tundra. *Nature*, 459, 556-559.

Schuur E.A.G., Crummer K.G., Vogel J.G. & Mack M.C. (2007). Plant species composition and productivity following permafrost thaw and thermokarst in Alaskan tundra. *Ecosystems*, 10, 280-292.

Sellers P. (1987). Canopy reflectance, photosynthesis and transpiration. II. The role of biophysics in the linearity of their interdependance. *International Journal of Remote Sensing*, 6, 1335-1372.

Serreze M. & Francis J.A. (2006). The arctic amplification debate. *Climate Change*, 76, 241-264.

Shaver G., Billings W.D., Chapin III F.S., Giblin A.E., Nadelhoffer K.J., Oechel W.C. & Rastetter E.B. (1992). Global change and the carbon balance of arctic ecosystems. *BioScience*, 42, 433-441.

Shur Y., Hinkel K.M. & Nelson F.E. (2005). The transient layer: implications for geocryology and climate-change science. *Permafrost and Periglacial Processes*, 16, 5-17.

Shur Y.L. & Jorgenson M.T. (2007). Patterns of permafrost formation and degradation in relation to climate and ecosystems. *Permafrost and Periglacial Processes*, 18, 7-19.

Sitch S., McGuire A.D., Kimball J., Gedney N., Gamon J., Engstrom R., Wolf A., Zhuang Q., Clein J. & McDonald K.C. (2007). Assessing the carbon balance of circumpolar Arctic tundra using remote sensing and process modeling. *Ecological Applications*, 17, 213-234.

Sitch S., Smith B., IPrentice I.C., Arneth A., Bondeau A., Cramer W., Kaplans J.O., Levis S., Lucht W., Sykes M.T., Thonicke K. & Venevsky S. (2003). Evaluation of ecosystem dynamics, plant geography and terrestrial carbon cycling in the LPJ dynamic global vegetation model. *Global Change Biology*, 9, 161-185.

Sjögersten S., van der Wal R. & Woodin S.J. (2008). Habitat type determines herbivory controls over CO2 fluxes in a warmer Arctic. *Ecology*, 89, 2103-2116.

Soegaard H., Nordstroem C., Frigorg T. & al. e. (2000). Trace gas exchange in a high-arctic valley. Integrating and scaling CO2 fluxes from canopy to landscape using flux data, footprint modeling, and remote sensing. *Global Biogeochemical Cycles*, 14, 725-744.

Soil Survey Staff (1999). Soil Taxonomy: A Basic System of Soil Classification for Making and Interpreting Soil Surveys. In: *Agricultural Handbook* Washington, D.C.

Stephens J. L., Boggs K., Garibaldi A., Grunblatt J. & Helt T. (2001). Denali National Park and Preserve landcover mapping project Volume 1: Remote sensing data, procedures and results. In: *National Resource Technical Report NPS/DENA/NRTR.* Fort Collins, Colorado: National Park Service.

Stieglitz M., Dery S.J., Romanovsky V.E. & Osterkamp T.E. (2003). The role of snow cover in the warming of Arctic permafrost. *Geophysical Research Letters*, 30.

Stow D., Hope A., McGuire D., Verbyla D., Gamon J., Huemmrich F., Houston S., Racine C., Sturm M., Tape K., Hinzman L., Yoshikawa K., Tweedie C., Noyle B., Silapaswan C., Douglas D., Griffith B., Jia G., Epstein H., Walker D., Daeschner S., Petersen A., Zhou L. & Myneni R. (2004). Remote sensing of vegetation and land-cover change in Arctic tundra ecosystems. *Remote Sensing Environment*, 89, 281-308.

Sturm M., Schimel J., Michaelson G., Welker J.M., Oberbauer S.F., Liston G.E., Fahnestock J. & Romanovsky V.E. (2005). Winter biological processes could help convert arctic tundra to shrubland. *BioScience*, 55, 17-26.

Sullivan P., Welker J.M., Arens S.J.T. & Sveinbjornsson B. (2008). Continuous estimates of CO2 efflux from arctic and boreal soils during the snow-covered season in Alaska. *Journal of Geophysical Research*, 113, G04009.

Taggeson T., Mastepanov M., Tamstorf M.P., Eklundh L., Schubert P., Ekberg A., Sigsgaard C., Christensen T.R. & Strom L. (2010). Satellites reveal an increase in gross primary production in a greenlandic high arctic fen 1992-2008. *Biogeosciences Discussions*, 7, 1101-1129.

Tarnocai C., Canadell J.G., Schuur E.A.G., Kuhry P., Mazhitova G. & Zimov S. (2009). Soil organic carbon pools in the northern circumpolar permafrost region. *Global Biogeochemical Cycles*, 23, 1-11.

Thornley J.H. & Johnson I.R. (1990). *Plant and Crop Modeling: A Mathmatical Approach to Plant and Crop Physiology*, Charldon, Oxford, U.K.

Trucco C., Schuur E.A.G., Natali S., Belshe E.F., Bracho R. & Vogel J. (2012). Long-term trends of CO2 exchange in a tundra ecoystem affected by permafrost thaw. *Journal of Geophysical Research-Biogeosciences*, 117.

Tucker C. (1979). Red and photographic infrared linear combinations for monitoring vegetation. *Remote Sensing Environ*, 8, 127-150.

Ueyama M., Iwata H., Harazono Y., Euskirchen E.S., Oechel W.C. & Zona D. (in press). Growing season and spatial variations of carbon fluxes of arctic and boreal ecosystems in Alaska. *Ecological Applications*.

van der Molen M.K., van Huissteden J., Parmentier F.J.W. & et al. (2007). The growing season greenhouse gas balance of a continental tundra site in the Indigirka lowlands, NE Siberia. *Biogeosciences*, 4.

Venables W. & Ripley B. (2002). *Modern Applied Statistics with S*. Fourth edn. Springer, New York, NY.

Vogel J., Schuur E., Trucco C. & Lee H. (2009). Response of CO2 exchange in a tussock tundra ecosystem to permafrost thaw and thermokarst development. *Journal of Geophysical Research*, 114.

Vourlitis G. & Oechel W. (1997). Landscape-scale CO 2, H 2 O vapour and energy flux of moist-wet coastal tundra ecosystems over two growing seasons. *Journal of Ecology*, 85, 575-590.

Vourlitis G., Verfaillie J., Oechel W., Hope A., Stow D. & Engstrom R. (2003). Spatial variation in regional CO2 exchange for the Kuparuk River Basin, Alaska over the summer growing season. *Global Change Biology*, 9, 930-941.

Vourlitis G.L., Harazono Y., Oechel W.C., Yoshimoto M. & Mano M. (2000a). Spatial and temporal variations in hectare-scale net CO 2 flux, respiration and gross primary production of Arctic tundra ecosystems. *Functional Ecology*, 14, 203-214.

Vourlitis G.L. & Oechel W.C. (1999). Eddy covariance measurements of CO2 and energy fluxes of an Alaskan tussock tundra ecosystem. *Ecology*, 80, 686-701.

Vourlitis G.L., Oechel W.C., Hope A., Stow D., Boynton B., Verfaillie Jr J., Zulueta R. & Hastings S.J. (2000b). Physiological models for scaling plot measurements of CO2 flux across an arctic tundra landscape. *Ecological Applications*, 10, 60-72.

Wahrhaftig C. (1958). Quarternary and engineering geology in the central part of the Alaska Range. *Geological Survey Professional Paper*, 293.

Walker D. A., Raynolds M. K., Daniels F. J. A., Einarsson E., Elvebakk A., Gould W. A., Katenin A. E., Kholod S. S., Markon C. J., Melnikov E. S., Moskalenko N. G., Talbot S. S., Yurtsev B. A. & other members of the CAVM team. (2005). The Circumpolar Arctic vegetation map. *Journal of Vegetation Science,* 16**,** 267-282.

Walter K.M., Smith S.L. & Chapin F.S. (2007). Methane bubbling from northern lakes: present and future contributions to the global methane budget. *Philosophical Transactions of the Royal Society A: Mathematical, Physical and Engineering Sciences.*, 365, 1657-1676.

Wang J., Sheng Y., Hinkel K.M. & Lyons L. (2012). Drained thaw lake basin recovery on the western Arctic Coastal Plain of Alaska using high-resolution digital elevation models and remote sensing imagery. *Remote Sensing of Environment*, 119, 325-336.

Webb E.K., Pearman G.I. & Leuning R. (1980). Correction of Flux Measurements for Density Effects Due to Heat and Water-Vapor Transfer. *Quarterly Journal of the Royal Meteorological Society*, 106, 85-100.

Welker J., Fahnestock J. & Jones M.H. (2000). Annual CO2 flux in dry and moist arctic tundra: field responses to increases in summer temperatures and winter snow depth. *Climatic Change*, 44.

Welker J.M., Brown K.B. & Fahnestock J. (1999). CO 2 flux in arctic and alpine dry tundra: comparative field responses under ambient and experimentally warmed conditions. *Arctic, Antarctic, and Alpine Research*, 31, 272-277.

Wickham H. (2009). *ggplot2: Elegant Graphics for Data Analysis*. Springer, New York.

Wilczak J., Oncley S. & Stage S. (2001). Sonic anemometer tilt correction algorithms. *Boundary-Layer Meteorol*, 99, 127-150.

Williams M., Bell R., Spadavecchia L., Street E. & Van Wijk M. (2008). Upscaling leaf area index in an Arctic landscape through multiscale observations. *Global Change Biology*, 14, 1517-1530.

Wood S. (2006). *Generalized Additive Models: An Introduction with R*. Chapman and Hall/CRC, Boca Raton.

Wood S.N. (2008). Fast stable direct fitting and smoothness selection for generalized additive models. *Journal of the Royal Statistical Scoiety (B)*, 70(3), 495-518.

Xu M. & Qi Y. (2001). Soil-surface CO2 efflux and its spatial and temporal variations in a young ponderosa pine plantation in northern California. *Global Change Biology*, 7, 667-677.

Yocum L., G.W. Adema & C.K. Hults (2006). A baseline study of permafrost in the Totlat Basin, Denali National Park and Preserve. In, pp. 37-40.

Yoshikawa K. & Hinzman L.D. (2003). Shrinking thermokarst ponds and groundwater dynamics in discontinuous permafrost near Council, Alaska. *Permafrost and Periglacial Processes*, 14.

Zamolodchikov D., Karelin D. & Ivaschenko A. (2000). Sensitivity of tundra carbon balance to ambient temperature. *Water, Air, And Soil Pollution*, 119, 157-169.

Zhang T., Barry RG, Knowles K, Heginbottom JA & Brown J (1999). Statistics and characteristics of permafrost and ground-ice distribution in the Northern Hemisphere. *Polar Geography*, 23, 132-154.

Zhang T., Frauenfeld O., Serreze M., Etringer A., Oelke C., McCreight J., Barry R., Gilichinsky D., Yang D. & Ye H. (2005). Spatial and temporal variability in active layer thickness over the Russian Arctic drainage basin. *J. Geophys. Res*, 110.

Zimov S., Davidov S., Voropaev Y., Prosiannikov S., Semiletov I., Chapin M. & Chapin F. (1996). Siberian CO2 efflux in winter as a CO2 source and cause of seasonality in atmospheric CO2. *Climatic Change*, 33, 111-120.

Zona D., Oechel W.C., Peterson K.M., Clements R.J., Paw K.T. & Ustin S.L. (2010). Characterization of the carbon fluxes of a vegetated drained lake basin chronosequence on the Alaskan Arctic Coastal Plain. *Global Change Biology*, 16, 1870-1882.

Zuur A., Ieno E., Walker N., Saveliev A. & Smith G. (2009). *Mixed Effects Models and Extensions in Ecology with R*. Springer, New York, NY.

BIOGRAPHICAL SKETCH

Fay Belshe grew up a poor Florida “cracker” and spent most of the days of her youth outdoors. Mostly, she was on the beach or in the shade of a large oak, trying to survive the summer heat. During this time she began to appreciate living things and wondered what created the beautiful patterns of nature. Although she would be lying if she said that from that point on her life was dedicated to ecological sciences. A lot of her years were spent drifting along, barely staying out of trouble. She finally became serious about school in the final years of her bachelor degree, when she studied horticultural sciences. After graduation, Fay continued studying plants in their natural environment and became interested in carbon cycling. During her master’s she examined the spatial and temporal variation of seagrass photosynthesis, which included many fun summers snorkeling in the Florida Keys. For her doctoral research, she expanded upon her knowledge of photosynthesis and focused on whole-ecosystem carbon cycling. Specifically, understanding and quantifying landscape patterns in carbon cycling created as permafrost thaws in an upland tundra ecosystem. It would be a second lie if she said she enjoyed working in high-latitude ecosystems, but she survived and got some pretty good data. Fay really enjoys the intricate patterns and stories that emerge from ecological data. By helping to tell the complex story of carbon, she hopes to contribute to the management of ecosystems in a warmer world. But beyond increasing knowledge within the scientific community, she hopes to tell a story about our understanding of the earth system that can reach the general public, and can change their conception of the importance of carbon in our climate.